Bioorg. Med. Chem. 37 (2021) 116109

Contents lists available at ScienceDirect

Bioorganic & Medicinal Chemistry

journal homepage: www.elsevier.com/locate/bmc

Twin drug design, synthesis and evaluation of diosgenin derivatives as multitargeted agents for the treatment of vascular dementia

Gui-Xiang Yang [a,1], Jia-Min Sun [a,1], Lu-Lu Zheng [a,1], Li Zhang [a], Jie Li [a], Hai-Xian Gan [a], Yan Huang [a], Jin Huang [a], Xing-Xing Diao [b], Yun Tang [a,*], Rui Wang [a,*], Lei Ma [a,*]

[a] Shanghai Key Laboratory of New Drug Design, School of Pharmacy, East China University of Science and Technology, 130 Meilong Road, Shanghai 200237, China
[b] Shanghai Institute of Materia Medica, Chinese Academy of Sciences, Shanghai 201203, China

ARTICLE INFO

Keywords:
Vascular dementia
Diosgenin
Antioxidant
Anti-cholinesterase
Multi-target-directed ligands

ABSTRACT

A novel series of multitargeted molecules were designed and synthesized by combining the pharmacological role of cholinesterase inhibitor and antioxidant of steroid as potential ligands for the treatment of Vascular Dementia (VD). The oxygen-glucose deprivation (OGD) model was used to evaluate these molecules, among which the most potent compound ML5 showed the highest activity. Firstly, ML5 showed appropriate inhibition of cholinesterases (ChEs) at orally 15 mg/kg in vivo. The further test revealed that ML5 promoted the nuclear translocation of Nrf2. Furthermore, ML5 has significant neuroprotective effect in vivo model of bilateral common carotid artery occlusion (BCCAO), significantly increasing the expression of Nrf2 protein in the cerebral cortex. In the molecular docking research, we predicted the ML5 combined with hAChE and Keap1. Finally, compound ML5 displayed normal oral absorption and it was nontoxic at 500 mg/kg, po, dose. We can draw the conclusion that ML5 could be considered as a new potential compound for VD treatment.

1. Introduction

Vascular Dementia (VD) is a neurodegenerative disease, which is related to various factors, including age, low levels of education, female sex, and vascular risk factors.[1] Recently, VD has become the main type of dementia except for Alzheimer's disease (AD), occupying roughly one-fifth of dementia.[2] Based on current research, VD has serious impacts on people's mental health and quality of life, the mortality and morbidity of VD are increasing as the population aging. There is no specific drug approved for anti-VD by the Food and Drug Administration (FDA) yet, although it can be delayed through early prevention.[3] Thus, it is necessary to develop new anti-VD drugs.

Acetylcholine (ACh), the first neurotransmitter identified in the central nervous system plays an important role in cognitive activities include learning, memory, and spontaneous behavior.[4,5] Damaged Cholinergic neurons in the brain is a characteristic of AD, VD, and other forms of dementia such as Lewy bodies dementia (LBD) and frontotemporal dementia (FTD).[6] AChE inhibitors can accumulate ACh at the synapse, prolong and increase the effects of ACh by inhibiting acetylcholinesterase (AChE). Currently, there are three AChE inhibitors used for the treatment of dementia, including donepezil, rivastigmine, galantamine.[7] Especially for AChE and butyryl cholinesterase (BuChE) inhibitory activity, rivastigmine has been approved by the FDA as a transdermal patch for the treatment of mild, moderate, and severe AD as well as mild-to-moderate Parkinson's disease dementia (PDD), and one research showed that rivastigmine had similar benefits to improving cognition and behavioral symptoms in patients with VD.[8]

VD is caused by a range of cardiovascular or cerebrovascular conditions, it can cause damages to learn and memory functions of the brain through pathways of inflammation and oxidative stress in blood vessels.[9,10] Nuclear factors erythroid 2-related factor 2 (Nrf2), a key transcription factor for the expression of the oxidative stress response is regulated by Kelch-like ECH-associated protein 1 (Keap1). The interaction between Nrf2 and the antioxidant reaction element (ARE) regulates the expression of antioxidant protein and phase II detoxifying enzyme.[11] Under normal circumstances, Nrf2 binds to Keap1 in the cytoplasm and the ubiquitination rapidly degrades.[12] When the level of oxidation beyond antioxidant capacity, the conformational change of Keap1 leads to cysteine residues being modified then the inherently

* Corresponding authors.
E-mail addresses: ytang234@ecust.edu.cn (Y. Tang), ruiwang@ecust.edu.cn (R. Wang), malei@ecust.edu.cn (L. Ma).
[1] These authors contributed equally to this work.

https://doi.org/10.1016/j.bmc.2021.116109
Received 15 January 2021; Received in revised form 1 March 2021; Accepted 6 March 2021
Available online 19 March 2021

combined Nrf2 was released to the nucleus.[13] Then, Nrf2 activated by binding to ARE in the nucleus, together with subsequent enhancement in the expression of its downstream antioxidant genes, including NADP(H) quinone oxidoreductase (NQO1) and heme oxygenase (HO-1).[11,14,15] Therefore, increasing Nrf2 stability through inhibiting the interaction between Nrf2 and Keap1 can increase antioxidants pathways.

Currently, the development of multitarget-directed drugs is considered the most efficient approach for diseases with complex etiology, particularly the neurodegenerative disorders.[16,17] In our previous work, we designed Sarsasapogenin derivatives AA13, AA36, and Diosgenin derivative M15 as antioxidants in neurodegenerative diseases.[18–20](Fig. 1) It is also reported that phenyl carbamate as potent cholinesterase inhibitors is often used in neuroprotective drug design.[21] For these purposes, we have selected twin drug strategy and steroid and phenyl carbamate to prepare multifunctional potent drugs for VD. In the present study, we designed 23 new compounds (ML1-ML23), next we summarized structure–activity relationships (SAR) on these compounds, obtained a new potent drug candidate for anti-VD. Especially compound ML5 fused rivastigmine and compound 3, which were pharmacophoric features of cholinesterase inhibition and antioxidant (Fig. 2).

Compound ML5 significantly increased cell viability against oxidative injuries stimulated by oxygen-glucose deprivation, and it also has a good ChEs inhibitory activity in vivo. Mechanistic studies revealed that compound ML5 was a potent Nrf2 activator to promote the nuclear translocation of Nrf2, which facilitates the expression of a series of Nrf2-driven antioxidant molecules, including superoxide dismutase (SOD) and glutathione (GSH). As a new potential drug candidate for the treatment of VD, ML5 showed strong antioxidant capacity, appropriate inhibition of ChEs, and induced neuroprotection following in vivo ischemia–reperfusion.

2. Results and discussion

2.1. Chemistry

The synthetic routes for compounds **ML1**-**ML23** were shown in Scheme 1. Compound **1**, 4,5-Didehydrotigogenone was obtained using Oppenauer oxidation methods began with commercially available Diosgenin. In the presence of tertbutyldimethylsilyl chloride (TBSCl), compound **1** reacted with 2,3-dicyano-5,6-dichlorobenzoquinone (DDQ) to produce compound **2** in 95% yield, which reacted to compound **3** with Li, diphenyl and diphenyl methane in tetrahydrofuran (THF). Compound **3**, Bis (trichloromethyl) Carbonate (BTC) and N,N-diisopropylethylamine (DIPEA) were stirred in DCM at 0 °C, followed by addition of different amines, which led to the produce of compounds **ML1**-**ML23**, as shown in Fig. 3.

2.2. Neuroprotection

Oxygen glucose deprivation (OGD) is one of the oxidative stress models, which was used to assess the antioxidant effects of compounds *in vitro*. Here, in order to evaluate the neuroprotection of compounds **ML1**-**ML23**, the antioxidant activities of target compounds were tested on SH-SY5Y cells against oxidative injuries stimulated by OGD. The level of cell viability was quantified by MTT assay, which was used to characterize the protective effect against OGD.

Compound treatment groups were treated with corresponding compounds while control and model cells were treated with medium for 2 h and then compound treatment cells and model cells were exposure to OGD for 4 h and reperfusion for 2 h. Control cells were incubated in the high-glucose medium and normal oxygen environment. As shown in Fig. 4, the model group had lower cell viability (OGD, 60.16%) compared with the control (100%, $p < 0.001$). In general, compounds **ML2**-**ML5**, **ML8**-**ML10**, **ML13** displayed high cell viability compared to the model. Compounds **ML2** (10–50 μM), **ML3** (100 μM), **ML4** (20–50 μM), **ML5** (1–50 μM), **ML6** (1 μM), **ML8** (10–50 μM), **ML9** (1–50 μM), **ML10** (100 μM), **ML12** (0.1–1 μM), **ML13** (1 μM), **ML14** (1–10 μM) and **ML15** (0.1–1 μM) significantly increased cell viability compared with model (Fig. 4, Fig. 1S, Supporting Information). In addition, at the indicated concentrations, some compounds shown in Fig. 4 have a tendency to increase cell viability in SH-SY5Y cells, but there was no statistical significance compared with the model. Compound **ML7** did not exhibit the effect to increase cell viability in the OGD model (Fig. 1S, Supporting Information). It was remarkable that the linear alkyl and branched alkyl carbamate derivatives **ML2**-**ML4** were much more effective in increasing the survival rate of the SH-SY5Y cells. In addition, **ML1** and **ML7**, bearing ethyl and 3-phenylpropyl, respectively, showed weaker neuroprotective abilities compared with compounds **ML2**-**ML4**. This demonstrated that introducing phenyl groups, which could strengthen the structural rigidity of the compound, would enhance the neuroprotective effect.

Disubstituted compounds **ML5** and **ML6** showed significant differences in the activity on OGD model, compound **ML5** with N-ethyl-N-methyl showed higher cell viability than **ML1** and **ML6** with N-ethyl and N, N-diethyl. **ML8** and **ML9** with cyclopentyl and cyclohexyl can afford neuroprotection, of which no clear SAR (structure–activity relationship) can be defined. Moreover, pyrrolidinyl substituted compound **ML10** showed higher cell viability than piperidyl substituted compound **ML11**, as shown in Figure 1S. It was notable that compounds **ML12**-**ML15** exhibited higher cell viability in OGD model of SH-SY5Y cells, which indicated that introducing substituted or unsubstituted benzyl carbamate would be beneficial to improve the activity of cytoprotective. However, when hetero atoms were introduced to the aryl substituents, compounds displayed potent inhibitory action at 10–100 μM. Cell viability was increased by the addition of compounds **ML19**-**ML23** at

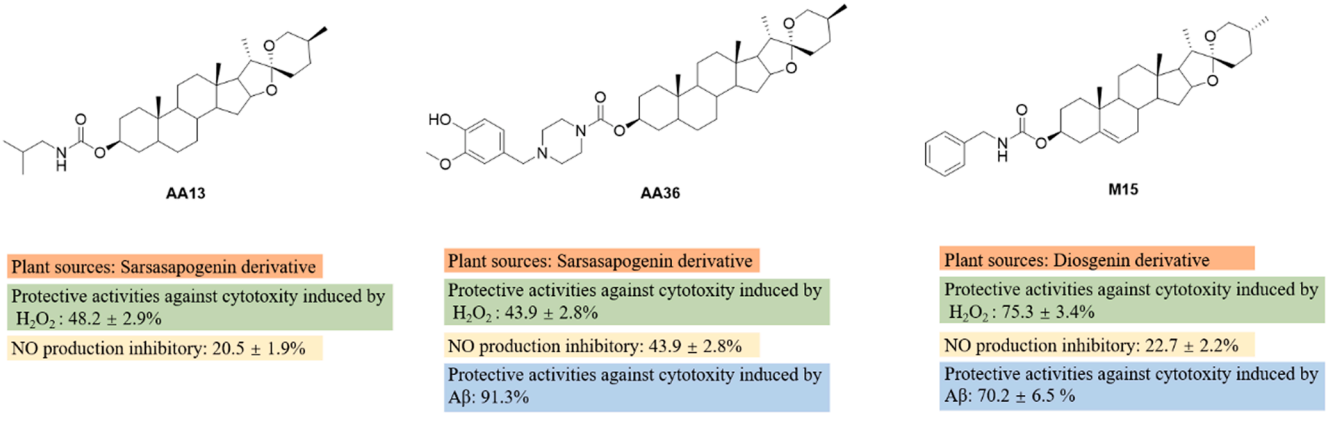

Fig. 1. The structure and protective activities of compounds **AA13**, **AA36** and **M15**.

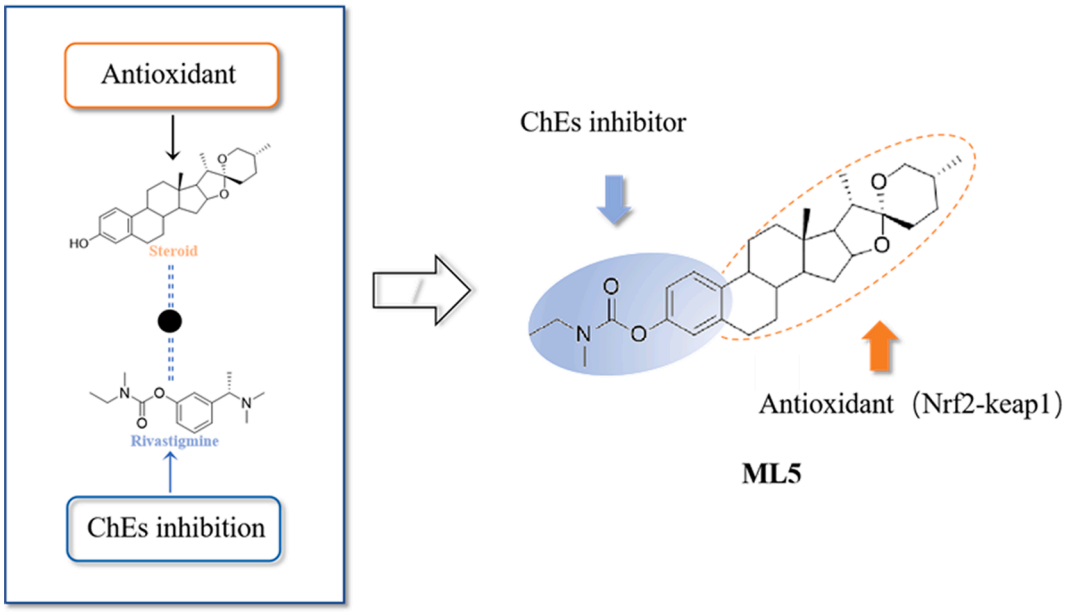

Fig. 2. Twin drug strategy design for multifunctional anti-VD agents.

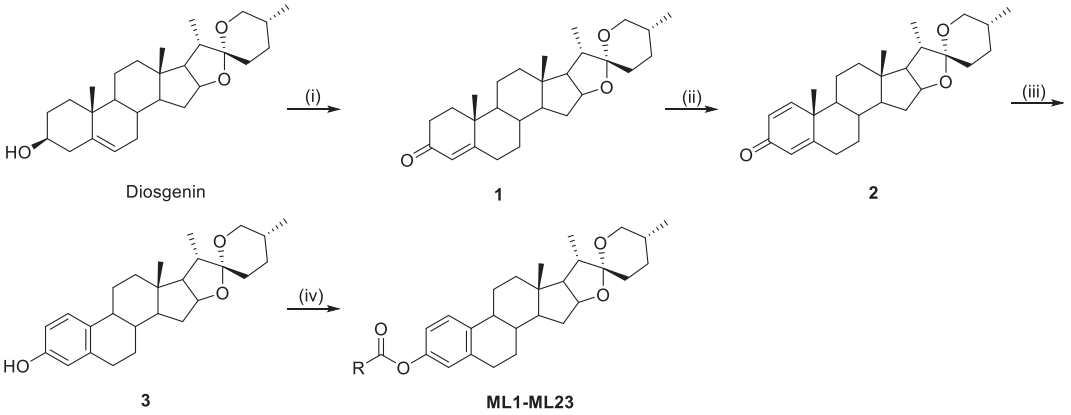

Scheme 1. Synthetic route of compound **1**, **2**, **3** and **ML1**-**ML23**. [a]Reagents and conditions: (i) aluminium isopropoxide, cyclohexanone, PhMe, 105 °C; (ii) DDQ, TBSCl, 1,4-dioxane, rt; (iii) Li, Diphenyl, Diphenyl methane, THF, 70 °C; (iv) BTC, amines, DIPEA, DCM, 0 °C.

low concentration compared with model while being below the model value at high concentration. Nevertheless, we have not found a clear SAR. In general, the neuroprotection of compounds was related to concentration, which displayed neuroprotection activity at low concentration and inhibitory effect at high concentration.

At last, we defined the neuroprotection activity as the percentage from model value, defined as 0%, to reach the control value, as 100% (Table 1). We found that most compounds emerged potent neuroprotection, especially the new phenyl carbamate **ML5**, providing strongest neuroprotective activity of 76.00 ± 4.02% cytoprotection rate at 10 μM (Table 1). In addition, **ML5** exhibited excellent bioactivities from 1 to 50 μM especially at low concentrations. Although some other compounds, such as **ML9**, similarly improve the cytoviabilities at 1 μM, their cytoprotectivity still not as good as **ML5** at each concentration. Then, we focused on **ML5** for its ChEs inhibitory activity.

2.3. *Effect of **ML5** on ChEs activity in vivo.*

The in vivo ChEs inhibitory activity of **ML5** was evaluated and compared with rivastigmine which was used as the positive controls (Fig. 5). The results showed that rivastigmine (2 mg/kg, i.g., dose) inhibited ChEs activity to 49.9% compared with the normal saline group in the mice cerebral cortex at 30 min after oral administration. At 15 min after gavage of 15 mg/kg **ML5**, the ChEs activity decreased to 76.3% compared with the normal saline group. The ChEs inhibition activity was strongest at 30 min after received **ML5** (64.6%) and lasted until 45 min (66.2%). The results showed that **ML5** significantly inhibited ChEs activity in the brain and provided evidence that **ML5** could cross the blood–brain barrier.

2.4. *ML5 prevented loss of cell viability and reduced ROS levels in SH-SY5Y cells exposed to H_2O_2*

Oxidative stress produced by reactive radical species has been recognized as a common pathological feature in VD. Reactive oxygen species (ROS), together with the loss of function of many antioxidant defense enzymes which could cause an imbalance between the formation of cellular oxidants and the antioxidative processes. First, we evaluated the cytoprotective effects of **ML5** at different concentrations (0.01–100 μM) on SH-SY5Y cells exposed to H_2O_2 at 200 μM using the 3-(4,5-dimethylthiazol-2-yl)-2,5-diphenyltetrazolium bromide (MTT) assay and ROS assay. As depicted in Figure 6A, the MTT assay indicated that H_2O_2 at 200 μM for 24 h induced a decrease in the viability of SH-SY5Y cell (77.8%) compared with control (100%, $p < 0.05$). However,

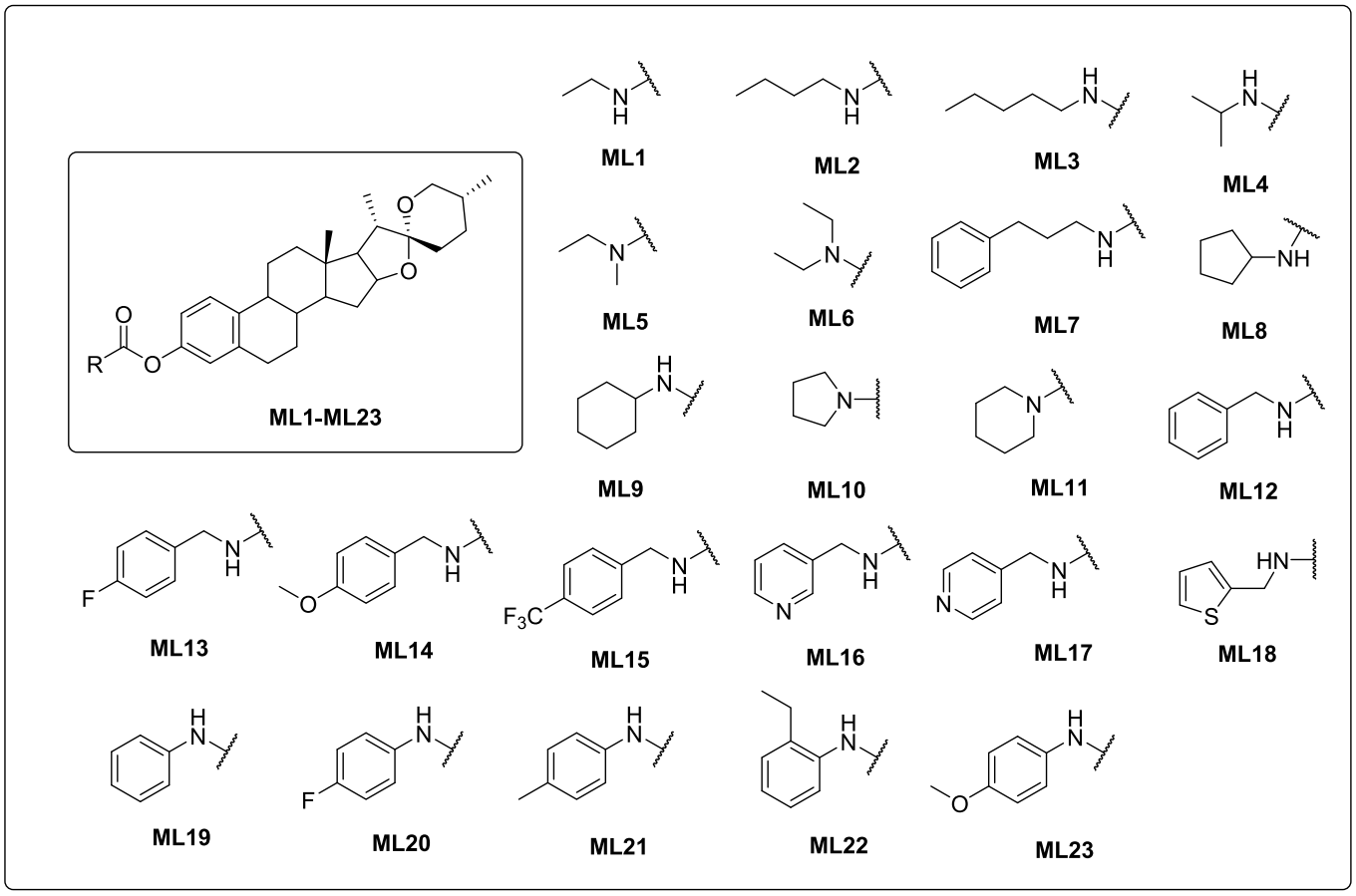

Fig. 3. Structures of the compounds **ML1**-**ML23**.

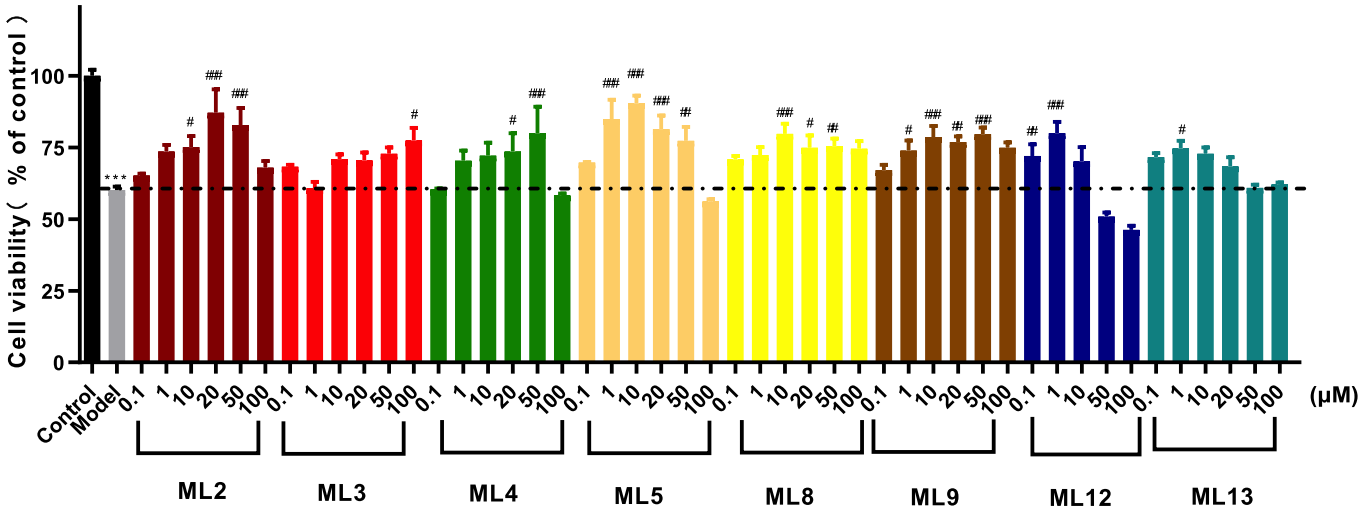

Fig. 4. Protection against Oxygen – Glucose Deprivation (OGD) of compounds **ML2**-**ML5**, **ML8**, **ML9**, **ML12**, **ML13**. Data are expressed in percentage with respect to 100% control. Data were expressed as mean ± SEM (n > 4). ***$p < 0.001$ compared with control group; #$p < 0.05$, ##$p < 0.01$, ###$p < 0.001$ compared with model group by one-way ANOVA analysis followed by a post hoc (Student-Newman-Keuls) test for multiple comparisons.

the H_2O_2-induced the decrease in cell viability was significantly attenuated when cells were pretreated with **ML5** for 2 h at 1 μM (87.7%), 5 μM (95.2%), 10 μM (96.5%) ($p < 0.05$). Based on these data, we decided to utilize the **ML5** at 1, 5, 10 μM in the next study.

We next studied whether **ML5** at 1, 5, 10 μM would be effective in decreasing ROS after 200 μM H_2O_2 stimulation. The 2′-7′dichlorofluorescin diacetate (DCFH-DA) is a non-fluorescent compound. This probe is cell-permeable and is hydrolyzed to the 2′-7′dichlorodihydrofluorescein (DCFH) carboxylate anion in the cell, which is retained in the cell. DCFH is later oxidized by intracellular ROS into 2′-7′dichlorofluorescein (DCF) which is a fluorescent compound. The fluorescence intensity can reflect ROS levels. Cells were pretreated with **ML5** for 2 h, and then 10 μM DCFH-DA was added, and followed by H_2O_2 (200 μM), then intracellular fluorescence intensity were analyzed

Table 1
Neuroprotection for compounds on SH-SY5Y cells after Oxygen-Glucose Deprivation (OGD).

Compd.	Conc. (μM)	Neuroprotection (%)
ML2	10	37.43 ± 2.02
	20	67.66 ± 6.10
	50	56.94 ± 4.73
ML3	100	43.36 ± 2.05
ML4	20	33.76 ± 3.46
	50	49.76 ± 5.14
ML5	1	62.07 ± 5.46
	10	76.00 ± 4.02
	20	53.38 ± 4.74
	50	43.16 ± 4.08
ML6	1	33.77 ± 3.32
ML8	10	49.20 ± 3.97
	20	37.07 ± 3.16
	50	38.30 ± 2.12
ML9	1	34.36 ± 2.30
	10	46.42 ± 2.72
	20	41.89 ± 1.61
	50	48.77 ± 1.91
ML10	100	37.77 ± 2.13
ML12	0.1	29.68 ± 2.65
	1	49.82 ± 3.92
ML13	1	36.41 ± 2.19
ML14	1	25.08 ± 5.95
	10	27.45 ± 8.18
ML15	0.1	20.43 ± 5.05
	1	25.93 ± 7.22

Neuroprotection was defined as the percentage from model value (defined as 0%) until reaching the control value (defined as 100%). Data were expressed as mean ± SEM (n > 4).

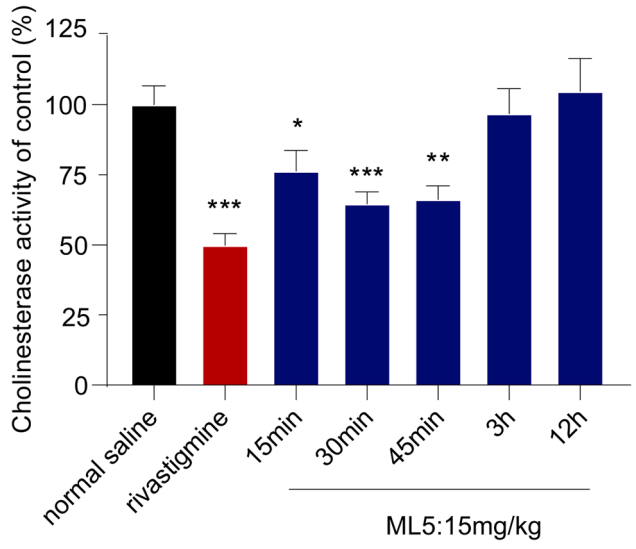

Fig. 5. Anti-ChEs activity of **ML5**. **ML5** inhibited ChEs activity significantly. Bar graph shows the cholinesterase activity after gavage administration of normal saline or rivastigmine 30 min and **ML5** 15 min, 30 min, 45 min, 3 h, 12 h, respectively. Cholinesterase activity of control brains were considered as 100% (black bar). Data are expressed in percentage with respect to 100% control. Data were expressed as mean ± SEM (n = 6 mice in each group, male). *$p < 0.05$, **$p < 0.01$, ***$p < 0.001$ compared with control group by one-way ANOVA analysis followed by a post hoc (Student-Newman-Keuls) test for multiple comparisons.

in a microplate reader and fluorescence microscope. As shown in Figure 6B, 30 min after H_2O_2 stimulation, the level of ROS in the H_2O_2 group increased to 141.8% compared to the control group (100%, $p < 0.05$). **ML5** at 1 μM was not effective in preventing the increased of ROS induced by H_2O_2, while 5 μM and 10 μM **ML5** significantly reduced ROS levels compared to the group treated with H_2O_2 alone (5 μM 114.2%, 10 μM 111.4%, $p < 0.05$). To further confirm the results of the ROS, we detected DCFH-DA green dye which, by fluorescence microscope, correlates a proportional green intensity to the quantity of ROS present in a cellular system. As shown in Figure 6C, the results were consistent with the quantitative results measured by the microplate reader. The fluorescence of the H_2O_2 group was stronger than that of the control group, and the fluorescence of the other three groups treated with **ML5** were decreased to some extent compared with H_2O_2 group.

These results and those described above showed that **ML5** induced a significant neuroprotective effect on neuronal cells subjected to H_2O_2, increased cell activity and decreased ROS.

2.5. *ML5 exerted antioxidant properties in H_2O_2-treated SH-SY5Y cells.*

ROS production is a consequence of the aerobic metabolism that is normally controlled by the endogenous antioxidant systems.[19] Living cells contain a large number of antioxidant species and antioxidant enzymes, both of which serve to counteracted harmful effects caused by free radicals.[22] GSH is a powerful antioxidant and SOD is one of the most important antioxidants enzymes.

The antioxidative effects of **ML5** were studied on SH-SH5Y cells by evaluating their SOD and GSH levels after pre-protected by **ML5** (1, 5, 10 μM) for 2 h and then exposed to 200 μM hydrogen peroxide for 24 h. As shown in Figure 7A and 7B, when treated with 200 μM H_2O_2 for 24 h, the activity of SOD of SH-SY5Y cells in the H_2O_2 group was significantly decreased to 50.7% than control ($p < 0.05$), and the GSH levels were significantly reduced to 74.4% compared with the control group ($p < 0.05$).

However, the SOD activities in cells that pretreated with 10 μM **ML5** for 2 h were significantly restored to 101.5% compared with the H_2O_2 group ($p < 0.05$), meanwhile pretreated with 1 μM and 5 μM **ML5** for 2 h, restored SOD activities to 82.7% and 83.3%, respectively, although the difference did not reach a statistical significance. The GSH levels in the cells pretreated with 10 μM **ML5** for 2 h were significantly restored to 93.6% compared with the H_2O_2 group ($p < 0.05$). The cells pretreated with 1 μM and 5 μM of **ML5** for 2 h restored the GSH levels to 81.5% and 91.0% respectively. These results indicated that **ML5** is effective to alleviate oxidative damage in SH-SY5Y cells induced by H_2O_2, which is mainly related to enhancing the activities of SOD and GSH.

2.6. *ML5 activated Nrf2 pathway in SY5Y cells*

Under normal physiological conditions, Nrf2 binds to Keap1 in the cytoplasm and degraded by programmed ubiquitination and proteasomal degradation, thus maintaining a low level. When Nrf2 pathway is activated, its translocation to the nucleus induces the expression of several genes implicated in antioxidant defences.[23]

We studied whether **ML5** would induce translocation of Nrf2 to the nucleus in SH-SY5Y cells by western blot analysis. As shown in Fig. 8, the result of western blot showed that 10 μM **ML5** significantly increased Nrf2 localization in the nucleus compared with that seen in the untreated control after 12 h treatment in SH-SY5Y cells.

2.7. *ML5 ameliorated learning and memory impairments, reduced neuronal loss in the hippocampus after bilateral common carotid artery occlusion (BCCAO)*

In the above experiments, we found that **ML5** has ChEs inhibitory activity and can protect the oxidative damage of H_2O_2 to SH-SY5Y cells. The hypothesis that chronic cerebral hypoperfusion contributes to the progression of dementia was proposed long ago, and recent studies have shown that hypoperfusion resulted in a chain of disruption of homeostatic interactions including oxidative stress.[24] Furthermore, substantial evidence has shown that 2VO can impair learning[25]. Therefore, we decided to assay **ML5** in animal models of BCCAO.

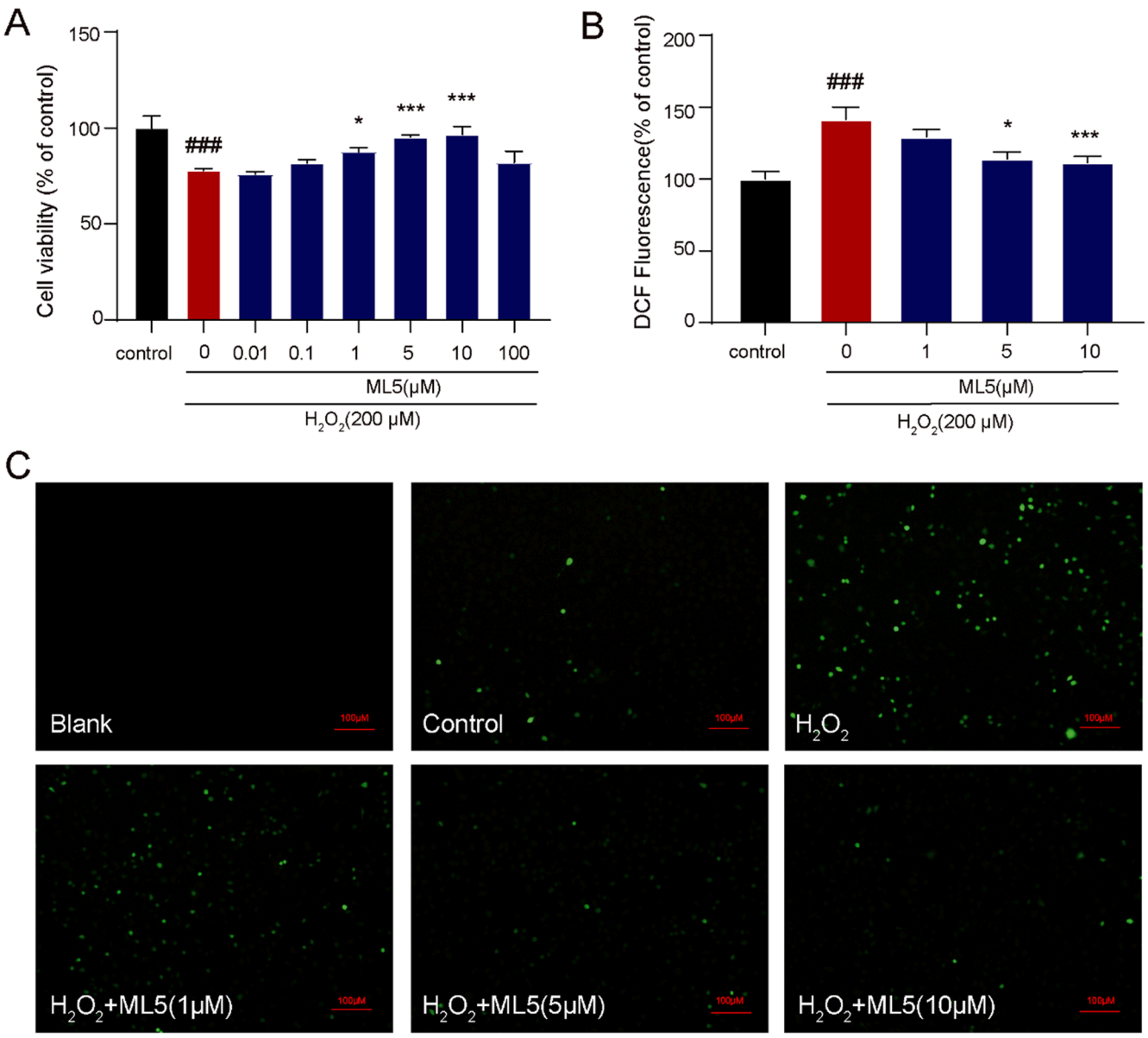

Fig. 6. Effect of **ML5** on cell viability of SH-SY5Y exposed to 200 μM H_2O_2. (A) Bar graph shows **ML5** pretreated at different concentrations (0.01–100 μM) for 2 h on the viability of SH-SY5Y cells exposed to 200 μM H_2O_2 for additional 24 h. Data are expressed as percentage with respect to the control which was presented as 100%. (B) Bar graph shows the effects of 2 h pretreatment of **ML5** at 1 μM, 5 μM, 10 μM on the cellular levels of reactive species generation, H_2O_2 was utilized at 200 μM for further 30 min (by microplate reader). ROS detected in control cells was considered as 100%. (C) The fluorescence images qualitatively show the intracellular ROS level after pretreatment with **ML5** at 1 μM, 5 μM, 10 μM for 2 h and 200 μM H_2O_2 for further 30 min (Fluorescence microscope shoot). Data were expressed as mean ± SEM (n = 3). #$p < 0.05$, ##$p < 0.01$, ###$p < 0.001$ compared with control; *$p < 0.05$, **$p < 0.01$, ***$p < 0.001$ compared with H_2O_2 group by one-way ANOVA analysis followed by a post hoc (Student-Newman-Keuls) test for multiple comparisons.

The Morris water maze is one of the most commonly used tests to measure the hippocampus-related spatial learning capacity in chronic cerebral hypoperfusion in rats. Therefore, we examined the learning and memory functions by analyzing escape latency and frequency in the platform quadrant using the Morris Water Maze test (MWM). SD rats were divided into sham operation, BCCAO, **ML5** low-dose (3 mg/kg, i.g.), **ML5** high-dose (15 mg/kg, i.g.), and donepezil (1 mg/kg, i.g.) groups, respectively. As shown in Figure 8D, the mean escape latency of all groups over the course of the 5 learning days decreased at 4 weeks after BCCAO.

The escape latency of the BCCAO group decreased slower than the sham group's during the training sessions, and during the probe trial phase, the BCCAO group stayed shorter in the target quadrant than the that in the sham group ($p < 0.05$, Figure 9B). Both of above-validated learning and memory deficits in our BCCAO rats. Importantly, the escape latency, either of **ML5** groups or the donepezil group, decreased faster than the BCCAO group (Figure 9A). In the probe trial, the group received **ML5** with a dose of 3, 15 mg/kg, and the group received donepezil 1 mg/kg stayed longer in the target quadrant than BCCAO group ($p < 0.05$, Figure 9B). At the same time, no statistical difference in swimming speed between any of the groups (Figure 9C). The specific movement trajectory of each group of rats was shown in Figure 9D. Figure 8E showed the overview of the hippocampal and enlarged views of CA1 regions by HE staining. The number of neurons in the sham group was higher than in other groups. Whether **ML5** treated groups or donepezil treated groups, the number of neurons was higher than the BCCAO groups, indicated that **ML5** treatment significantly reduced the loss of neurons after BCCAO. These results suggested that **ML5** would

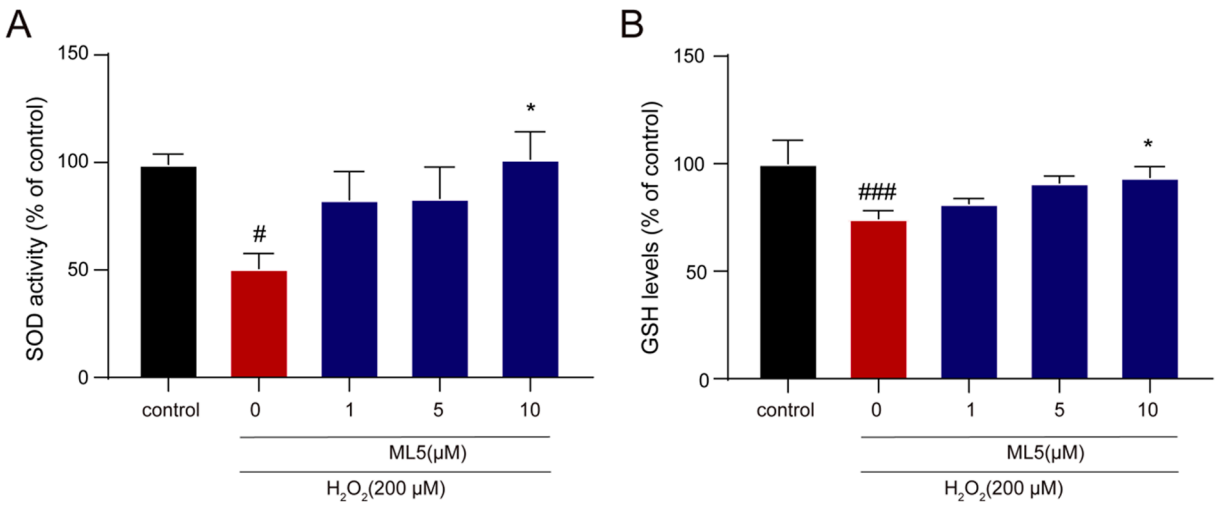

Fig. 7. The effects of **ML5** on the levels of SOD and GSH in SH-SY5Y cells treated with 200 μM H_2O_2. (A) Bar graph shows the activity of SOD in SH-SY5Y cells after **ML5** pretreatment at 1, 5, 10 μM for 2 h and exposed to 200 μM H_2O_2 for additional 24 h. (B) Bar graph shows the level of GSH in SH-SY5Y cells after **ML5** pretreatment at 1, 5, 10 μM for 2 h and exposed to 200 μM H_2O_2 for additional 24 h. Data are expressed in percentage with respect to 100% control. Data were expressed as mean ± SEM (n = 3–5). $\#p < 0.05$, $\#\#p < 0.01$, $\#\#\#p < 0.001$ compared with control; $^*p < 0.05$, $^{**}p < 0.01$, $^{***}p < 0.001$ compared with H_2O_2 group by one-way ANOVA analysis followed by a post hoc (Student-Newman-Keuls) test for multiple comparisons.

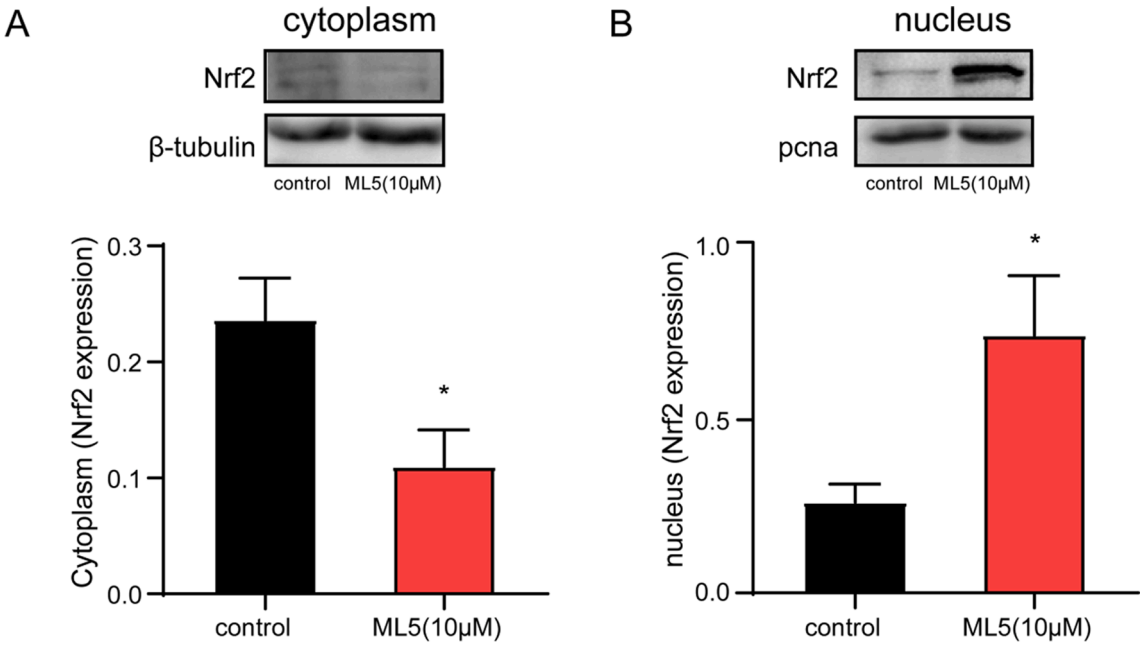

Fig. 8. Compound **ML5** activates Nrf2 pathway. (A) Western blot analyses of cytoplasm Nrf2 protein content from SH-SY5Y cells treated for 12 h with 10 μM **ML5** (n = 5) and relative expression levels of cytoplasm Nrf2. (B) Western blot analyses of nucleus Nrf2 protein content from SH-SY5Y cells treated for 12 h with 10 μM **ML5** (n = 5) and relative expression levels of nucleus Nrf2. Data were expressed as mean ± SEM (n = 5). $\#p < 0.05$, $\#\#p < 0.01$, $\#\#\#p < 0.001$ compared with control; $^*p < 0.05$, $^{**}p < 0.01$, $^{***}p < 0.001$ compared with control group by one-way ANOVA analysis followed by a post hoc (Student-Newman-Keuls) test for multiple comparisons.

mitigate the learning and memory deficits caused by BCCAO.

2.8. *ML5 exerted an antioxidant and neuroprotective effect by activating Nrf2 pathway.*

Transcription factor Nrf2 is the main protein that regulates oxidative stress in the body and it is a transcription factor that induces the expression of a great number of cytoprotective and detoxification genes.[26] There are pieces of evidence that Keapl-Nrf2-ARE signal pathway is the most important signal pathway in the body to resist excessive ROS and maintain redox homeostasis, as it reduces oxidative stress and neuroinflammation. Therefore, the Nrf2 pathway is being increasingly considered a therapeutic target for Neurodegenerative disease.

In our above research, we found that **ML5** could reverse the increase of ROS and the decrease of SOD and GSH caused by H_2O_2 damage in SH-SY5Y cells. Therefore, we decided to explore whether the neuroprotective effect of **ML5** on BCCAO rats is related to its antioxidant capacity and whether it is achieved by activating the Nrf2 pathway. We then tested the SOD activity and GSH content in the cerebral cortex of each group of rats to observe whether ML5 alleviated oxidative damage in BCCAO rats.

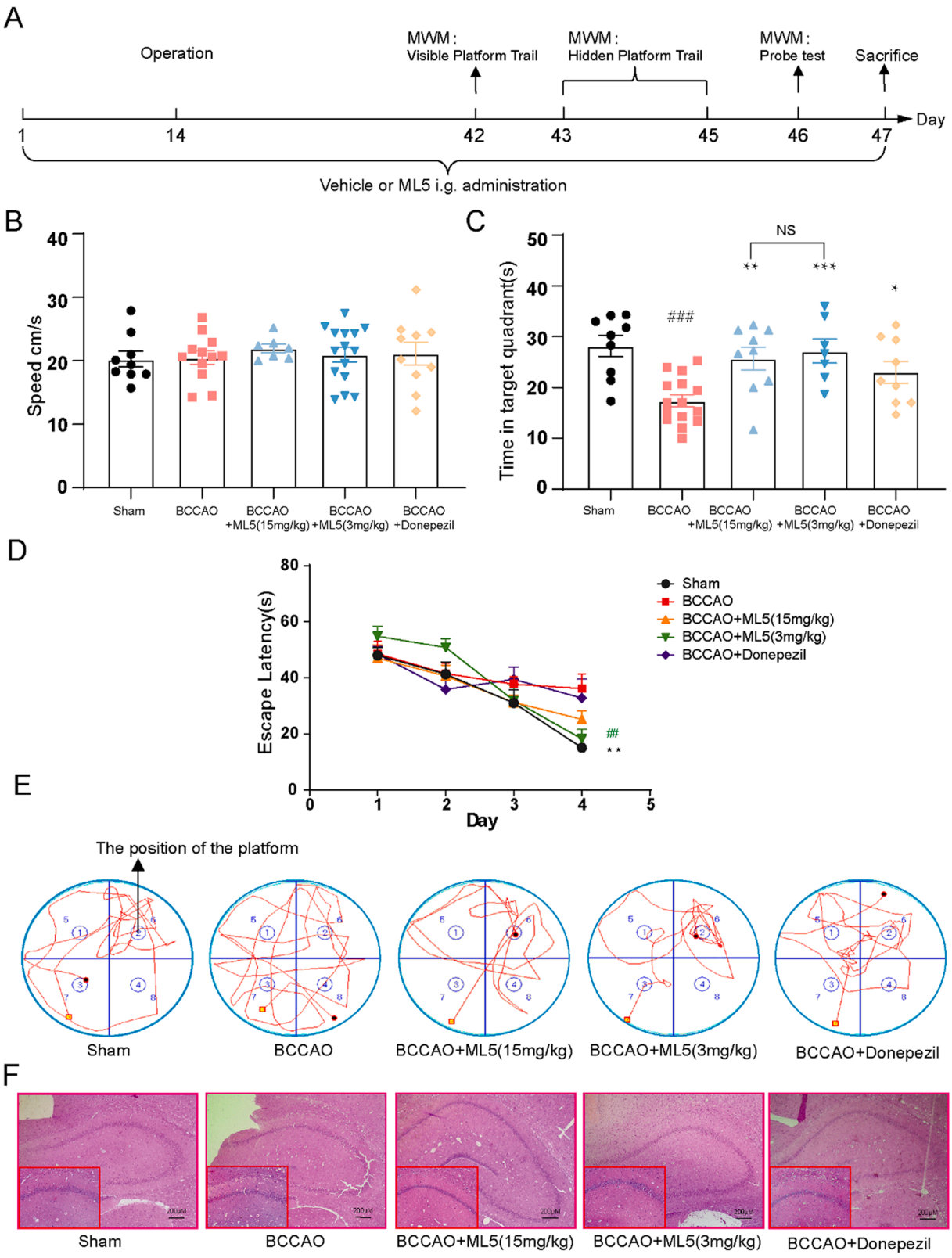

Fig. 9. Neuroprotective effect and cognitive recovery of **ML5** on BCCAO rats. (A) Timeline of **ML5** treatment and behavioral assessment. Mice were treated with **ML5** (4 mg/kg or 20 mg/kg) two week prior to the beginning of behavioral testing and treatment continued throughout the experiment. After testing, animals were sacrificed and tissue was harvested. **ML5** treatment lasted a total of 46 days. (B) Bar graph shows the quantitative analysis of the mean speed in 1 min at day 5 of MWM test between the different groups. (C) Bar graph shows the time spent in the target quadrant in the probe trial. (D) Line chart shows the escape latency changes in the different groups from days 1 to 5 of MWM test. (E) Representative photographs of probe test in the WMW test. (F) Representative photographs of HE staining (magnification: ×40) in the hippocampal and the enlarged CA1 region (magnification: ×100). Data are presented as mean ± SEM; n = 8–13. $\#p < 0.05$, $\#\#p < 0.01$, $\#\#\#p < 0.001$ compared with sham; $^{*}p < 0.05$, $^{**}p < 0.01$, $^{***}p < 0.001$ compared with BCCAO group by one-way ANOVA analysis followed by a *post hoc* (Student-Newman-Keuls) test for multiple comparisons.

As shown in Figure 10A-B, the SOD activity and GSH levels of BCCAO group were decreased to 59.8% and 60.6% severally compared with control ($p < 0.05$). **ML5** suppressed the BCCAO-induced reduction in the activity of the SOD and the levels of GSH. The SOD activity of the 3 mg/kg treatment group (85.9%) and the 15 mg/kg (98.4%) treatment group was significantly higher than that of the BCCAO surgery group (both $p < 0.05$). In addition, the GSH level in the 15 mg/kg (81.4%) treatment group was also significantly higher than the BCCAO surgery group, but the GSH level in the 3 mg/kg treatment group (68%) was not significantly recovered due to the larger standard error.

Aiming to investigate the mechanism underlying the antioxidant stress and neuroprotective effects of **ML5**, we examined the protein expression level of Nrf2 in the cerebral cortex. The Western blot results revealed that **ML5** treatment significantly increased the expression of Nrf2 protein in the cerebral cortex compared with the BCCAO group ($p < 0.05$). Therefore, the antioxidant and neuroprotective effects of compound **ML5** are closely related to the activation of Nrf2.

2.9. Insights into bioactive mechanisms

Given that **ML5** possesses potent inhibitory activities targeting hAChE (PDB ID: 6F25) compared with its counterpart rivastigmine, molecular docking studies were performed to compare their potential bioactive mechanisms. There are five substrate-binding regions in the active site gorge of hAChE, including catalytic triad residues, oxyanion hole, anionic site (AS), acyl pocket, and peripheral anionic site (PAS).[27] As shown in Figure 11A, both **ML5** and rivastigmine could properly occupy the active site gorge of hAChE. As for **ML5** (Figure 11B), its phenyl carbamate moiety goes deeply into the PAS region of hAChE. The carbonyl group of phenyl carbamate moiety forms a stable hydrogen bond interaction with TYR 124. The π-π stacking interaction formed by benzene ring of **ML5** and TRY 341 further stabilizes the binding of **ML5** to hAChE. Due to the traction of cation-π interaction formed by TRY 286 and protonated nitrogen, the pose of rivastigmine is rotated by about 90°compared to **ML5** (Figure 11A and C). Nevertheless, the interactive features of the phenyl carbamate portion of rivastigmine are extremely similar to that of **ML5**. TYR 124 forms a hydrogen bond interaction with the oxygen atom of the phenyl ester group. The π-π stacking interaction is also conserved by interacting with PHE 338, which could reinforce the interaction between rivastigmine and hAChE. In addition, **ML5** and rivastigmine can act on AS region TRP 86 via hydrophobic interaction. The MM-GBSA ΔGbinding values for **ML5** and rivastigmine with hAChE are −63.166 kcal/mol and −56.262 kcal/mol, respectively. The binding affinity of **ML5** is slightly superior to that of rivastigmine, probably because **ML5** could be stabilized by a hydrophobic hole composed of residues located at the entrance of an active site gorge, such as HIS 287, TRP 286, and GLU 292. It is evidenced that PAS (TYR 72, ASP 74, TYR 124, TRP 286) and AS (TRP 86) are promising binding sites for the treatment of AD and TYR 124 is a significant anchoring point for the binding of small molecular inhibitors.[27,28] The strong interactions between **ML5** with PAS and AS, especially with PAS, combined with the superior binding affinity between **ML5** and hAChE would guarantee **ML5** as a bioactive molecule with effective neuroprotection.

The Keap1 (PDB ID: 3VNH) plays a key role in the negative regulation of Nrf2-mediated cytoprotective response. C-terminal Kelch domain of Keap1 is a recognition module for Nrf2 and inhibition of Kelch-Nrf2 interaction is recognized as an effective strategy for the therapy of neurodegenerative diseases.[29,30] We docked **ML5** to the Kelch domain of Keap1 to investigate its potential bioactive mechanism. As illustrated in Fig. 12, **ML5** is properly anchored into the Kelch domain of Keap1 with MM-GBSA ΔGbinding = −49.683 kcal/mol. The oxygen atom of phenyl

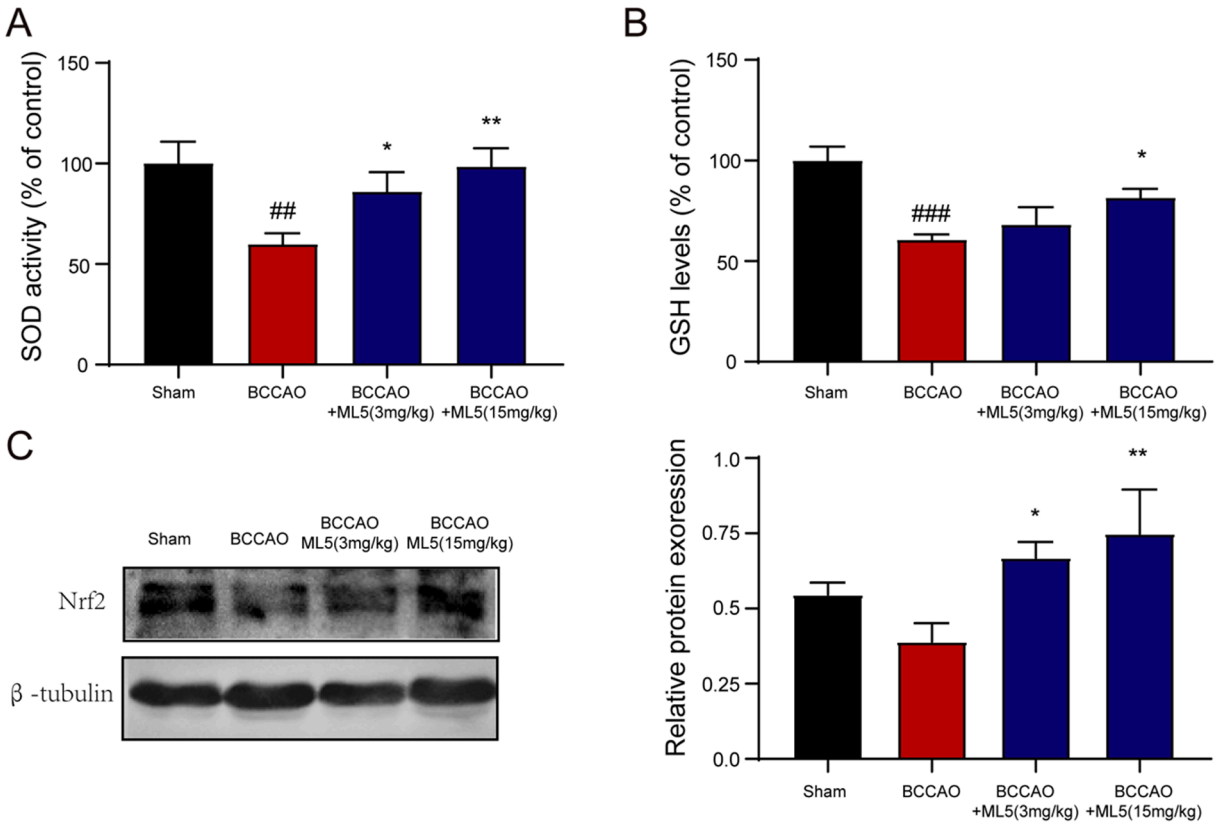

Fig. 10. The effects **ML5** on the levels of antioxidants and the expression of Nrf2 in BCCAO rats. (A) Bar graph shows the activity of SOD in all groups at 4 weeks after BCCAO. (B) Bar graph shows the levels of GSH in all groups at 4 weeks after BCCAO. (C) Quantitative analysis of the western blotting shows the Nrf2 expression levels in the cortex of all groups. Data are presented as mean ± SEM; n = (8–13). #$p < 0.05$, ##$p < 0.01$, ###$p < 0.001$ compared with sham; *$p < 0.05$, **$p < 0.01$, ***$p < 0.001$ compared with BCCAO group by one-way ANOVA analysis followed by a post hoc (Student-Newman-Keuls) test for multiple comparisons.

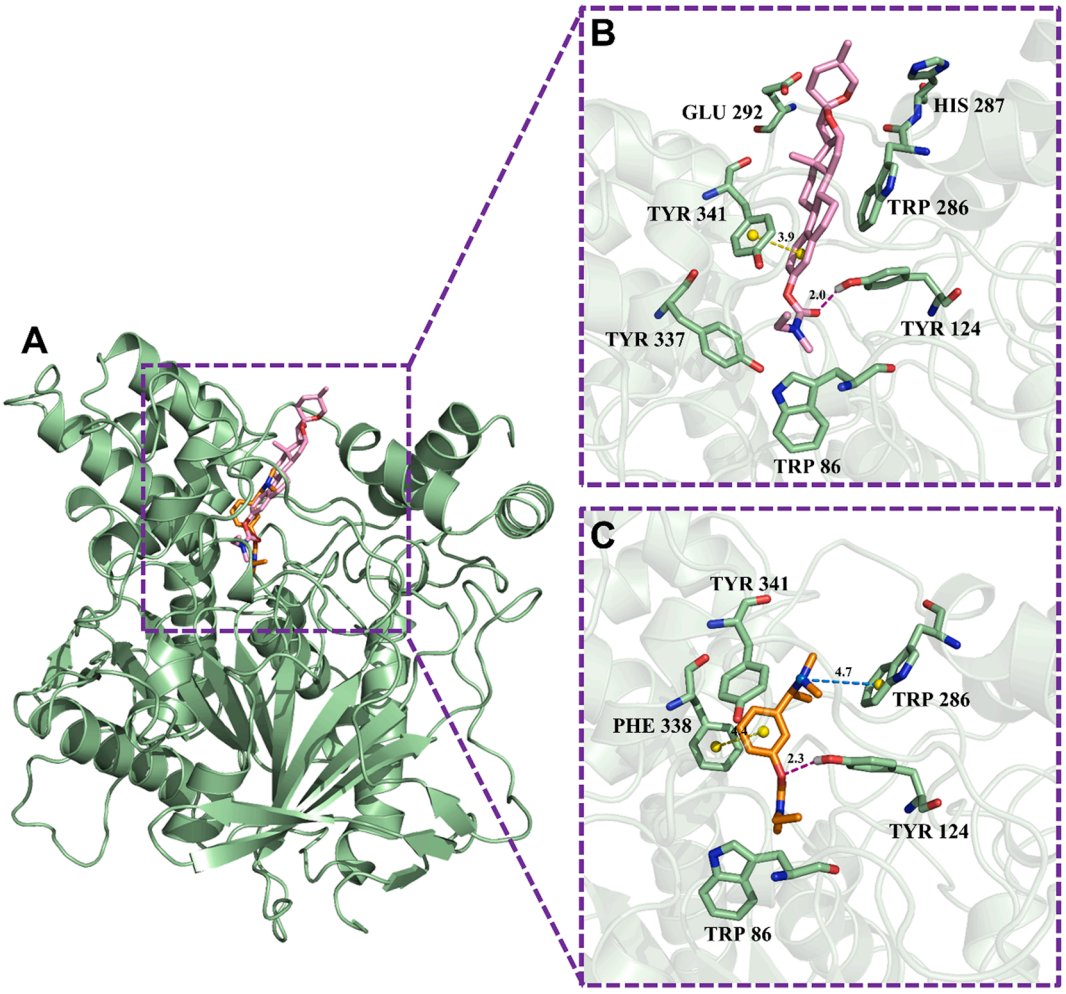

Fig. 11. The alignment of docking poses of **ML5** and rivastigmine (A), binding models of **ML5** (B) and rivastigmine (C) interacting with hAChE (PDB ID: 6F25). Proteins are shown as green cartoons. Small molecules and key residues are drawn as sticks. Carbons in **ML5**, rivastigmine and key residues are colored in pink, orange and green, respectively. All oxygen, nitrogen and hydrogen (polar hydrogen only) atoms are colored in red, blue and white, respectively. Aromatic ring centers and positron centers are presented as yellow and blue spheres. Hydrogen bonds, π-π stacking interactions and cation-π bonds are depicted in purple, yellow and cyan dotted lines, respectively.

carbamate moiety directly interacts with SER 602 and forms a stable hydrogen bond with its hydroxy group. Moreover, the tail tetrahydropyran group is toward the edge of the active site and interacts with ASN 382 by hydrogen bond interaction. The benzene ring of **ML5** forms a π-π interaction with TYR 334, which would effectively stabilize the binding of **ML5** into Keap1. In addition, hydrophobic interaction stemmed from ARG 380 and ARG 415 contributes to the molecular binding to some extent. Shih-Ching Lo et al.3 found that residues ARG 380, ASN 382, and ARG 415 of Keap1 participate in hydrogen bond interactions with the side chain atoms of Nrf2, and residues in Keap1 including TYR 334, ASN 382, and SER 602 participate in hydrogen bonding interactions with the backbone of Nrf2. The mutagenesis analysis of Keap1 showed that mutation of individual residues for ARG 380, TYR 334, ASN 382 and ARG 415 significantly disrupts the capability of Keap1 binding to Nrf2, and these residues are required for repression of Nrf2-dependent transcription. Therefore, **ML5** could firmly occupy the Kelch domain of Keap1, which would interfere with the recognition between Keap1 and Nrf2, thus exert promising neuroprotective activity.

2.10. Acute toxicity study

These studies indicated that compound **ML5** had obviously anti-VD effect in vivo and *in vitro*. Acute toxicity study is considered to be an essential basis for the safety evaluation of new drugs. Therefore, the most promising drug candidate **ML5** was selected to study its acute toxicity by oral administration at a dose of 500 mg/kg (n = 7). All the animals were observed for 14 days after administration. After observation, all the animals were alive and performed healthily from the color of their fur, weight changes, behavioral symptoms, water, and food consumption. All mice were sacrificed on the 15th day to observe the changes in the heart, liver, and kidneys. All organs observed were normal. This result displayed that **ML5** had well-tolerated at a dose of 500 mg/kg with no acute toxicity.

3. Conclusions

We designed, synthesized and biologically evaluated 23 new candidate compounds for VD treatment, which fused steroid and phenyl carbamate together according to our previous work. Some of the test compounds (**ML2**, **ML3**, **ML4**, **ML5**, **ML6**, **ML8**, **ML9**, **ML10**, **ML12**, **ML13**, **ML14** and **ML15**) significantly increased cell viability with the OGD model. Among the series, compound **ML5** showed the highest neuroprotection activity in the OGD model and appropriate inhibition of ChEs at oral 15 μM in vivo, which indicated ROS scavenging and cell viability increasing against SH-SY5Y cells damage induced by H_2O_2. Further pharmacological experiments showed that **ML5** could promote Nrf2 nuclear translocation and hence promote the levels of SOD and GSH, affording protection of SH-SY5Y cells from oxidative insults. In the

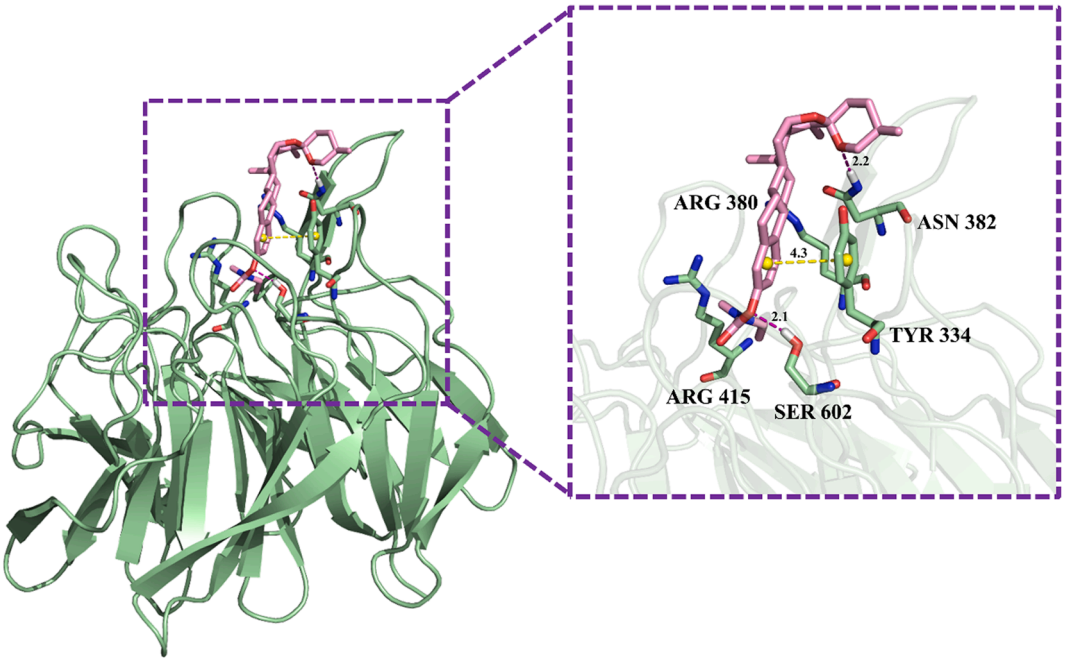

Fig. 12. Predicted binding model of **ML5** interacting with Keap1 (PDB ID: 3VNH). Painting rules are the same as mentioned in Fig. 11.

BCCAO-induced VD model, **ML5** mitigated the learning and memory deficits, which significantly reversed the BCCAO-induced loss of neurons and improved the levels of SOD and GSH in the hippocampus. In the molecular studies, **ML5** exhibited good binding affinity in the active site of AChE and firmly occupied the Kelch domain of Keap1, which would interfere with the recognition between Keap1 and Nrf2, thus exert promising neuroprotective activities. In addition, **ML5** was found to be well-tolerated and nontoxic up to 500 mg/kg, po, dose. Put all together, the most promising multitargeted drug **ML5** could be deemed as a potential drug in anti-VD for further study.

4. Experimental section

4.1. General

Reagents and solvents were purchased from common commercial suppliers, which were not treated further, unless specified. Reactions were detected by TLC (Yantai Huanghai, China) and tested with UV light ($\lambda = 254$ nm) or 1% vanillin sulfuric acid solution. Products were purified by chromatographic separations (200–300 mesh), which were produced from Yantai Huanghai, China. ^{1}H spectra were recorded by a Bruker AV-400 instrument in $CDCl_3$ with tetramethylsilane (TMS, Me_4Si) as an internal standard. ^{1}H spectra were expressed by δ (ppm), *J*, spin multiplicities. ^{13}C spectra were recorded by Ascend-600 instrument in $CDCl_3$ which were characterized by δ (ppm). High-resolution mass (HRMS, ESI) spectral data were acquired by ABSCIEX 4600 TOF electrospray mass spectrometer in positive ion mode.

Compounds **ML1-23** were analyzed by HPLC to determine their purity. The analyses were performed on Agilent 1260 series HPLC system (C-18 column, Shimadzu, 5 μm, 4.6 mm × 150 mm) at room temperature. The HPLC chromatograms of compounds **ML1-23** are included in the Supporting Information. All the tested compounds were dissolved in acetonitrile. Acetonitrile and water (98:2) were used as mobile phase, and the flow rate was set at 0.6 mL/min. The maximal absorbance at the range of 203 nm was used as the detection wavelength. The purity of compounds **ML1-ML23** was determined by the HPLC analysis (>95%), which meets the purity requirement by the Journal.

4.2. General method for synthesis of compound *1*

In a 500 mL round bottomed flask, the diosgenin (82.46 g, 0.2 mol), aluminium isopropoxide (1.5 equiv), and cyclohexanone (1.5 equiv) were suspended in 300 mL toluene. The mixture was stirred for 4 h at 90 °C until the reaction was completed according to TLC detection. The toluene was removed under reduced pressure. The residue was dissolved in dichloromethane, filtered with Buchner funnel. The filtrate was dried with Na_2SO_4 and concentrated under vacuum. The mixture was purified on a silica gel column using mixtures of ethyl acetate/petroleum ether = 1:20 as eluent, obtaining the corresponding compound **1** as a white amorphous powder.

4.3. General method for synthesis of compound *2*

Chlorotrimethylsilane (543.2 mg, 0.05 equiv) was added slowly to a solution of compound **1** (41.03 g, 0.1 mol) in tetrahydrofuran and 1,4-dioxane (200 mL, V_{THF}/V_{DO} = 1/1) at 0 °C. Then, 2,3-dicyano-5,6-dichlorobenzoquinone (1.5 equiv) was added. After 12 h of reaction, the mixture was diluted with water, extracted with DCM, dried over anhydrous sodium sulfate, filtered and the solvent evaporated. The resultant crude mixture was isolated by column chromatography using mixed eluent (ethyl acetate/petroleum ether = 1:15), the compound **2** was acquired as a white amorphous powder.

4.4. General method for synthesis of compound *3*

In a 250 mL double-neck flask, lithium metallic block (9.92 g, 1.43 mol), biphenyl (58.6 g, 380 mmol) and diphenyl methane (28.5 mL) were suspended in 300 mL dry THF under N_2 atmosphere. The mixture was reacted at 70 °C for 30 min until mixed system had turned blue. Then, the solution of compound **2** (95 mmol) was added. After the reaction was complete (detected by TLC), the mixture was cooled to room temperature before adjust the pH by adding 10% aq. HCl and extracted with DCM. The organic layer was dried with Na_2SO_4 and concentrated under vacuum. The compound **3** was obtained by column chromatography using ethyl acetate/petroleum ether = 1:20 as eluent.

4.5. General method for synthesis of compounds *ML1*-*ML23*

Compound **3** (184.6 mg, 0.5 mmol) and bis(trichloromethyl)carbonate (59.4 mg, 0.2 mmol) were dissolved in dry DCM under N_2 atmosphere at 0 °C. After 30 min of reaction, the different amines (1.5 equiv) were added. TLC was used to determine the reaction end point. Then, diluted the mixture with water, washed with brine, dried over Na_2SO_4, concentrated under vacuum and isolated by column chromatography. At last, we obtained products **ML1**-**ML23**.

ML1: White amorphous powder, yield 93%. ^{1}H NMR (400 MHz, $CDCl_3$) δ 7.24 (1H, d, J = 8.5 Hz), 6.87 (1H, dd, J = 8.2 Hz, 1.8 Hz), 6.83 (1H, s), 4.94 (1H, t, J = 5.2 Hz), 4.46 (1H, m), 3.49 (1H, dd, J = 10.1 Hz, 4.5 Hz), 3.39 (1H, t, J = 10.9 Hz), 3.31 (2H, m), 2.85 (2H, m), 1.21 (3H, t, J = 7.3 Hz), 1.00 (3H, d, J = 6.7 Hz), 0.80 (6H, m); ^{13}C NMR (151 MHz, $CDCl_3$) δ 154.80, 148.76, 137.96, 137.50, 126.07, 121.61, 118.66, 109.30, 80.84, 66.89, 62.30, 55.35, 43.93, 41.64, 40.76, 39.91, 38.05, 36.10, 31.56, 31.41, 30.31, 29.50, 28.80, 27.73, 26.31, 17.17, 16.40, 15.15, 14.52. HRMS (ESI): Calcd for $C_{29}H_{42}NO_4$ $[M+H]^+$ 468.3114; Found: 468.3096.

ML2: White amorphous powder, yield 91%. ^{1}H NMR (400 MHz, $CDCl_3$) δ 7.23 (1H, d, J = 8.8 Hz), 6.85 (1H, d, J = 8.7 Hz), 6.82 (1H, s), 4.46 (1H, dd, J = 14.8 Hz, 5.6 Hz), 3.58 (2H, m), 3.49 (3H, m), 3.39 (1H, t, J = 11.2 Hz), 2.85 (2H, m), 1.00 (3H, d, J = 6.7 Hz), 0.80 (6H, m); ^{13}C NMR (151 MHz, $CDCl_3$) δ 154.92, 148.79, 137.94, 137.47, 126.06, 121.59, 118.64, 109.29, 80.84, 66.88, 62.30, 55.35, 43.94, 41.64, 40.95, 40.77, 39.91, 38.05, 31.92, 31.57, 31.41, 30.31, 29.50, 28.81, 27.74, 26.31, 19.91, 17.14, 16.40, 14.52, 13.74. HRMS (ESI): Calcd for $C_{31}H_{46}NO_4$ $[M+H]^+$ 496.3427; Found: 496.3419.

ML3: White amorphous powder, yield 90%. ^{1}H NMR (400 MHz, $CDCl_3$) δ 7.24 (1H, d, J = 8.5 Hz), 6.87 (1H, d, J = 8.4 Hz), 6.84 (1H, s), 4.95 (1H, t, J = 5.8 Hz), 4.46 (1H, dd, J = 13.5 Hz, 7.4 Hz), 3.49 (1H, dd, J = 11.6 Hz, 2.8 Hz), 3.39 (1H, t, J = 10.9 Hz), 3.25 (2H, dd, J = 13.4 Hz, 6.8 Hz), 2.87 (2H, m), 1.00 (3H, d, J = 6.7 Hz), 0.92 (3H, t, J = 6.7 Hz), 0.80 (6H, m); ^{13}C NMR (151 MHz, $CDCl_3$) δ 154.91, 148.79, 137.94, 137.46, 126.05, 121.59, 118.64, 109.29, 80.84, 66.88, 62.30, 55.35, 43.94, 41.64, 41.24, 40.77, 39.91, 38.05, 31.57, 31.41, 30.31, 29.53, 29.50, 28.90, 28.81, 27.74, 26.31, 22.34, 17.15, 16.40, 14.52, 14.00. HRMS (ESI): Calcd for $C_{32}H_{48}NO_4$ $[M+H]^+$ 510.3583; Found: 510.3577.

ML4: White amorphous powder, yield 89%. ^{1}H NMR (400 MHz, $CDCl_3$) δ 7.24 (1H, d, J = 8.5 Hz), 6.87 (1H, d, J = 8.4 Hz), 6.84 (1H, s), 4.80 (1H, d, J = 7.5 Hz), 4.46 (1H, m), 3.89 (1H, dd, J = 13.5 Hz, 6.8 Hz), 3.49 (1H, dd, J = 10.1 Hz, 3.3 Hz), 3.39 (1H, t, J = 10.9 Hz), 2.86 (2H, m), 1.23 (6H, d, J = 6.5 Hz), 1.00 (3H, d, J = 6.8 Hz), 0.80 (6H, m); ^{13}C NMR (151 MHz, $CDCl_3$) δ 154.04, 148.76, 137.94, 137.45, 126.06, 121.64, 118.70, 109.30, 80.85, 66.90, 62.32, 55.36, 43.95, 43.39, 41.66, 40.78, 39.93, 38.07, 31.58, 31.42, 30.32, 29.51, 28.82, 27.75, 26.32, 22.95, 17.16, 16.41, 14.54. HRMS (ESI): Calcd for $C_{30}H_{44}NO_4$ $[M+H]^+$ 482.3270; Found: 482.3252.

ML5: White amorphous powder, yield 90%. ^{1}H NMR (400 MHz, $CDCl_3$) δ 7.24 (1H, d, J = 8.5 Hz), 6.86 (1H, d, J = 8.4 Hz), 6.82 (1H, s), 4.45 (1H, m), 3.49 (1H, m), 3.43 (1H, m), 3.39 (1H, t, J = 8.4 Hz), 3.01 (3H, s), 2.86 (2H, m), 1.00 (3H, d, J = 6.8 Hz), 0.81 (3H, s), 0.80 (3H, d, J = 6.5 Hz); ^{13}C NMR (151 MHz, $CDCl_3$) δ 154.92, 149.25, 137.87, 137.31, 126.01, 121.68, 118.77, 109.26, 80.83, 66.87, 62.31, 55.35, 44.01, 43.93, 41.64, 40.76, 39.92, 38.07, 34.21, 31.57, 31.41, 30.31, 29.49, 28.80, 27.75, 26.32, 17.14, 16.40, 14.52, 13.19. HRMS (ESI): Calcd for $C_{30}H_{44}NO_4$ $[M+H]^+$ 482.3270; Found: 482.3257.

ML6: White amorphous powder, yield 87%. ^{1}H NMR (400 MHz, $CDCl_3$) δ 7.24 (1H, d, J = 8.5 Hz), 6.86 (1H, d, J = 8.5 Hz), 6.83 (1H, s), 4.45 (1H, m), 3.49 (1H, d, J = 6.9 Hz), 3.39 (5H, m), 2.87 (2H, m), 1.00 (3H, d, J = 6.7 Hz), 0.80 (6H, m); ^{13}C NMR (151 MHz, $CDCl_3$) δ 154.53, 149.24, 137.84, 137.23, 125.99, 121.68, 118.76, 109.27, 80.84, 66.88, 62.31, 55.36, 43.93, 42.17, 41.82, 41.64, 40.76, 39.92, 38.09, 31.57, 31.41, 30.31, 29.49, 28.80, 27.76, 26.33, 17.15, 16.40, 14.53, 14.23, 13.42. HRMS (ESI): Calcd for $C_{31}H_{46}NO_4$ $[M+H]^+$ 496.3427; Found: 496.3405.

ML7: White amorphous powder, yield 84%. ^{1}H NMR (400 MHz, $CDCl_3$) δ ^{1}H NMR (400 MHz, $CDCl_3$) δ 7.27 (5H, m), 7.13 (1H, d, J = 8.7 Hz), 6.62 (1H, dd, J = 8.4 Hz, 2.5 Hz), 6.56 (1H, s), 4.70 (1H, s), 4.45 (1H, m), 3.90 (1H, t, J = 7.8 Hz), 3.60 (2H, m), 3.49 (1H, d, J = 5.9 Hz), 3.39 (1H, t, J = 10.8 Hz), 2.83 (2H, m), 1.00 (3H, d, J = 6.8 Hz), 0.82 (3H, s), 0.80 (3H, d, J = 6.3 Hz); ^{13}C NMR (151 MHz, $CDCl_3$) δ 153.64, 145.03, 138.10, 132.46, 128.41(2C), 127.81(2C), 126.29, 126.09, 115.26, 112.64, 109.46, 80.94, 66.89, 62.84, 62.22, 55.30, 51.34, 43.73, 41.65, 40.80, 39.91, 38.34, 35.46, 32.63, 31.49, 31.36, 30.27, 29.56, 28.74, 27.86, 26.44, 24.24, 17.13, 16.42, 14.50. HRMS (ESI): Calcd for $C_{36}H_{48}NO_4$ $[M+H]^+$ 558.3583; Found: 558.3585.

ML8: White amorphous powder, yield 87%. ^{1}H NMR (400 MHz, $CDCl_3$) δ 7.24 (1H, d, J = 8.3 Hz), 6.87 (1H, d, J = 8.4 Hz), 6.84 (1H, s), 4.91 (1H, d, J = 7.5 Hz), 4.46 (1H, m), 4.05 (1H, dd, J = 14.1 Hz, 7.0 Hz), 3.49 (1H, dd, J = 8.3 Hz, 3.9 Hz), 3.42 (1H, t, J = 6.7 Hz), 2.87 (2H, m), 1.00 (3H, d, J = 6.7 Hz), 0.80 (6H, m). ^{13}C NMR (151 MHz, $CDCl_3$) δ 154.33, 148.77, 137.90, 137.41, 126.03, 121.61, 118.67, 109.28, 80.83, 66.87, 62.30, 55.35, 52.95, 43.93, 41.64, 40.76, 39.91, 38.05, 33.17 (2C), 31.56, 31.41, 30.31, 29.49, 28.80, 27.74, 26.31, 23.55 (2C), 17.15, 16.39, 14.52. HRMS (ESI): Calcd for $C_{32}H_{46}NO_4$ $[M+H]^+$ 508.3427; Found: 508.3412.

ML9: White amorphous powder, yield 93%. ^{1}H NMR (400 MHz, $CDCl_3$) δ ^{1}H NMR (400 MHz, $CDCl_3$) δ 7.23 (1H, d, J = 8.3 Hz), 6.87 (1H, d, J = 8.5 Hz), 6.83 (1H, s), 4.87 (1H, d, J = 7.6 Hz), 4.45 (1H, m), 3.56 (1H, dd, J = 10.9 Hz, 6.9 Hz), 3.49 (1H, dd, J = 10.3 Hz, 3.2 Hz), 3.39 (1H, t, J = 10.9 Hz), 2.86 (2H, m), 1.00 (3H, d, J = 6.7 Hz), 0.80 (6H, d, J = 8.5 Hz); ^{13}C NMR (151 MHz, $CDCl_3$) δ 153.98, 148.78, 137.87, 137.35, 126.00, 121.59, 118.65, 109.27, 80.83, 66.87, 62.30, 55.34, 50.04, 43.93, 41.64, 40.75, 39.91, 38.05, 33.26 (2C), 31.56, 31.40, 30.30, 29.49, 28.80, 27.74, 26.30, 25.47, 24.76 (2C), 17.14, 16.39, 14.52. HRMS (ESI): Calcd for $C_{33}H_{48}NO_4$ $[M+H]^+$ 522.3583; Found: 522.3576.

ML10: White amorphous powder, yield 84%. ^{1}H NMR (400 MHz, $CDCl_3$) δ 7.24 (1H, d, J = 8.5 Hz), 6.88 (1H, dd, J = 8.4 Hz, 2.3 Hz), 6.85 (1H, s), 4.45 (1H, m), 3.54 (2H, t, J = 6.5 Hz), 3.48 (3H, m), 3.39 (1H, t, J = 10.9 Hz), 2.87 (2H, m), 1.00 (3H, d, J = 6.7 Hz), 0.81 (H, s), 0.80 (3H, d, J = 6.5 Hz); ^{13}C NMR (151 MHz, $CDCl_3$) δ 153.51, 149.15, 137.84, 137.25, 125.99, 121.71, 118.76, 109.28, 80.85, 66.88, 62.31, 55.36, 46.40, 46.31, 43.94, 41.64, 40.77, 39.93, 38.07, 31.57, 31.41, 30.32, 29.51, 28.81, 27.77, 26.32, 25.82, 24.99, 17.15, 16.41, 14.53. HRMS (ESI): Calcd for $C_{31}H_{44}NO_4$ $[M+H]^+$ 494.3270; Found: 494.3248.

ML11: White amorphous powder, yield 92%. ^{1}H NMR (400 MHz, $CDCl_3$) δ 7.23 (1H, d, J = 8.4 Hz), 6.86 (1H, d, J = 8.4 Hz), 6.83 (1H, s), 4.95 (1H, t, J = 5.6 Hz), 4.45 (1H, m), 3.48 (1H, m), 3.39 (1H, t, J = 10.9 Hz), 3.26 (2H, dd, J = 13.2 Hz, 6.7 Hz), 2.85 (2H, m), 1.00 (3H, d, J = 6.7 Hz), 0.95 (4H, t, J = 7.3 Hz), 0.80 (6H, m); ^{13}C NMR (151 MHz, $CDCl_3$) δ 154.09, 149.28, 137.85, 137.27, 126.00, 121.72, 118.77, 109.26, 80.84, 66.87, 62.31, 55.36, 45.46, 45.03, 43.93, 41.64, 40.76, 39.92, 38.06, 31.57, 31.41, 30.31, 29.49, 28.80, 27.76, 26.31, 25.92, 25.52, 24.34, 17.15, 16.40, 14.53. HRMS (ESI): Calcd for $C_{32}H_{46}NO_4$ $[M+H]^+$ 508.3427; Found: 508.3423.

ML12: White amorphous powder, yield 94%. ^{1}H NMR (400 MHz, $CDCl_3$) δ 7.33 (5H, m), 7.24 (1H, d, J = 8.6 Hz), 6.89 (1H, d, J = 8.4 Hz), 6.86 (1H, s), 5.29 (1H, t, J = 5.7 Hz), 4.45 (3H, d, J = 5.9 Hz), 3.49 (1H, dd, J = 10.6 Hz, 3.9 Hz), 3.39 (1H, t, J = 10.9 Hz), 2.86 (2H, m), 1.00 (3H, d, J = 6.7 Hz), 0.81 (3H, s), 0.80 (3H, d, J = 6.5 Hz); ^{13}C NMR (151 MHz, $CDCl_3$) δ 154.99, 148.73, 138.10, 138.02, 137.65, 128.77 (2C), 127.73 (2C), 127.68, 126.11, 121.56, 118.61, 109.30, 80.84, 66.89, 62.30, 55.35, 45.34, 43.94, 41.65, 40.77, 39.91, 38.04, 31.57, 31.41, 30.32, 29.51, 28.81, 27.73, 26.31, 17.15, 16.40, 14.53. HRMS (ESI): Calcd for $C_{34}H_{44}NO_4$ $[M+H]^+$ 530.3270; Found: 530.3252.

ML13: White amorphous powder, yield 89%. ^{1}H NMR (400 MHz, $CDCl_3$) δ 7.32 (2H, dd, J = 8.2 Hz, 5.5 Hz), 7.24 (1H, d, J = 8.6 Hz), 7.04 (2H, t, J = 8.5 Hz), 6.88 (1H, d, J = 8.6 Hz), 6.85 (1H, s), 5.29 (1H, t, J = 5.6 Hz), 4.46 (1H, m), 4.41 (2H, d, J = 5.9 Hz), 3.49 (1H, dd, J = 11.0 Hz, 3.1 Hz), 3.39 (1H, t, J = 10.9 Hz), 2.87 (2H, m), 1.00 (3H, d, J = 6.7

Hz), 0.80 (6H, m); ^{13}C NMR (151 MHz, $CDCl_3$) δ 162.28 (d, J = 245.7 Hz), 154.98, 148.66, 138.05, 137.72, 133.95 (d, J = 3.6 Hz), 129.44 (d, J = 8.1 Hz, 2C), 126.12, 121.53, 118.58, 115.58 (d, J = 21.8 Hz, 2C), 109.29, 80.82, 66.88, 62.29, 55.34, 44.60, 43.93, 41.64, 40.75, 39.90, 38.03, 31.56, 31.40, 30.30, 29.50, 28.80, 27.71, 26.30, 17.14, 16.39, 14.52. HRMS (ESI): Calcd for $C_{34}H_{43}FNO_4$ $[M+H]^+$ 548.3176; Found: 548.3170.

ML14: White amorphous powder, yield 88%. ^{1}H NMR (400 MHz, $CDCl_3$) δ 7.26 (3H, m), 6.89 (3H, m), 6.85 (1H, s), 5.21 (1H, s), 4.45 (1H, m), 4.38 (2H, d, J = 5.8 Hz), 3.81 (3H, s), 3.49 (1H, dd, J = 10.0 Hz, 3.2 Hz), 3.39 (1H, t, J = 10.8 Hz), 2.87 (2H, m), 1.00 (3H, d, J = 6.7 Hz), 0.80 (6H, m); ^{13}C NMR (151 MHz, $CDCl_3$) δ 159.15, 154.92, 148.74, 137.99, 137.59, 130.23, 129.14 (2C), 126.08, 121.57, 118.62, 114.11 (2C), 109.29, 80.83, 66.88, 62.30, 55.34, 55.31, 44.80, 43.93, 41.64, 40.76, 39.90, 38.04, 31.56, 31.41, 30.31, 29.50, 28.80, 27.72, 26.31, 17.14, 16.39, 14.52. HRMS (ESI): Calcd for $C_{35}H_{46}NO_5$ $[M+H]^+$ 560.3376; Found: 560.3361.

ML15: White amorphous powder, yield 90%. ^{1}H NMR (400 MHz, $CDCl_3$) δ 7.62 (2H, d, J = 7.9), 7.47 (2H, d, J = 8.0), 7.24 (1H, d, J = 8.6 Hz), 6.89 (1H, d, J = 8.4 Hz), 6.86 (1H, s), 5.41 (1H, t, J = 6.1 Hz), 4.47 (3H, m), 3.49 (1H, dd, J = 10.1 Hz, 3.2 Hz), 3.39 (1H, t, J = 10.9 Hz), 2.87 (2H, m), 1.00 (3H, d, J = 6.7 Hz), 0.80 (6H, m); ^{13}C NMR (151 MHz, $CDCl_3$) δ 155.11, 148.60, 142.25, 138.11, 137.83, 129.92(q, J = 32.9 Hz), 127.85 (2C), 126.16, 125.70 (2C), 125.67, 121.49, 118.54, 109.30, 80.83, 66.89, 62.30, 55.34, 44.77, 43.93, 41.65, 40.76, 39.89, 38.03, 31.56, 31.41, 30.31, 29.50, 28.81, 27.70, 26.31, 17.14, 16.39, 14.52. HRMS (ESI): Calcd for $C_{35}H_{43}F_3NO_4$ $[M+H]^+$ 598.3144; Found: 598.3144.

ML16: White amorphous powder, yield 84%. ^{1}H NMR (400 MHz, $CDCl_3$) δ 8.57 (2H, m), 7.72 (1H, d, J = 7.8 Hz), 7.30 (1H, dd, J = 7.7 Hz, 5.0 Hz), 7.24 (1H, d, J = 8.6 Hz), 6.88 (1H, d, J = 8.5 Hz), 6.85 (1H, s), 5.44 (1H, t, J = 5.9 Hz), 4.47 (3H,m), 3.49 (1H, dd, J = 10.9 Hz, 4.0 Hz), 3.39 (1H, t, J = 10.9 Hz), 2.86 (2H, m), 1.00 (3H, d, J = 6.7 Hz), 0.80 (6H, m); ^{13}C NMR (151 MHz, $CDCl_3$) δ 155.17, 149.07, 148.97, 148.59, 138.07, 137.79, 135.66, 133.91, 126.14, 123.63, 121.50, 118.55, 109.29, 80.81, 66.87, 62.28, 55.32, 43.91, 42.76, 41.63, 40.74, 39.88, 38.01, 31.54, 31.39, 30.29, 29.48, 28.79, 27.69, 26.29, 17.14, 16.38, 14.52. HRMS (ESI): Calcd for $C_{33}H_{43}N_2O_4$ $[M+H]^+$ 531.3223; Found: 531.3208.

ML17: White amorphous powder, yield 87%. ^{1}H NMR (400 MHz, $CDCl_3$) δ 8.59 (2H, d, J = 5.1 Hz), 7.28 (3H, m), 7.25 (1H, d, J = 8.6 Hz), 6.90 (1H, dd, J = 8.3 Hz, 2.0 Hz), 6.86 (1H, s), 5.48 (1H, t, J = 6.1 Hz), 4.46 (3H, m), 3.49 (1H, dd, J = 10.0 Hz, 3.1 Hz), 3.39 (1H, t, J = 10.9 Hz), 2.88 (2H, m), 1.00 (3H, d, J = 6.7 Hz), 0.81 (3H, s), 0.80 (3H, d, J = 6.5 Hz); ^{13}C NMR (151 MHz, $CDCl_3$) δ 155.21, 149.92 (2C), 148.56, 147.44, 138.13, 137.89, 126.18, 122.23 (2C), 121.45, 118.50, 109.30, 80.82, 66.88, 62.29, 55.33, 44.07, 43.92, 41.64, 40.75, 39.88, 38.02, 31.55, 31.40, 30.30, 29.50, 28.80, 27.70, 26.30, 17.14, 16.39, 14.52. HRMS (ESI): Calcd for $C_{33}H_{43}N_2O_4$ $[M+H]^+$ 531.3223; Found: 531.3208.

ML18: White amorphous powder, yield 86%. ^{1}H NMR (400 MHz, $CDCl_3$) δ 7.25 (1H, d, J = 7.6 Hz), 7.03 (1H, d, J = 2.7 Hz), 6.98 (1H, dd, J = 5.0 Hz, 3.5 Hz), 6.89 (1H, dd, J = 8.4 Hz, 2.2 Hz), 6.85 (1H, s), 5.33 (1H, t, J = 5.7 Hz), 4.62 (2H, d, J = 5.8 Hz), 4.45 (1H, m), 3.49 (1H, dd, J = 10.1 Hz, 3.2 Hz), 3.39 (1H, t, J = 10.9 Hz), 2.88 (2H, m), 1.00 (3H, d, J = 6.8 Hz), 0.81 (3H, s), 0.80 (3H, d, J = 6.5 Hz); ^{13}C NMR (151 MHz, $CDCl_3$) δ 154.65, 148.65, 140.71, 138.05, 137.72, 126.98, 126.14, 126.12, 125.36, 121.54, 118.59, 109.30, 80.84, 66.89, 62.30, 55.35, 43.94, 41.65, 40.76, 40.05, 39.90, 38.04, 31.57, 31.41, 30.31, 29.50, 28.81, 27.72, 26.31, 17.15, 16.40, 14.53. HRMS (ESI): Calcd for $C_{32}H_{42}NO_4S$ $[M+H]^+$ 536.2835; Found: 536.2833.

ML19: White amorphous powder, yield 91%. ^{1}H NMR (400 MHz, $CDCl_3$) δ 7.44 (2H, d, J = 7.7 Hz), 7.34 (2H, t, J = 7.9 Hz), 7.28 (1H, d, J = 8.5 Hz), 6.94 (1H, dd, J = 8.4 Hz, 2.4 Hz), 6.90 (1H, d, J = 2.2 Hz), 4.46 (1H, m), 3.49 (1H, d, J = 8.0 Hz), 3.40 (1H, t, J = 10.9 Hz), 2.89 (2H, m), 1.00 (3H, d, J = 6.7 Hz), 0.82 (3H, s), 0.80 (3H, d, J = 6.3 Hz); ^{13}C NMR (151 MHz, $CDCl_3$) δ 151.91, 148.26, 138.18, 138.03, 137.51, 129.13 (2C), 128.63, 126.22, 123.79, 121.61, 118.63 (2C), 109.32, 80.84, 66.89, 62.29, 55.34, 43.94, 41.65, 40.76, 39.90, 38.02, 31.56, 31.41, 30.31, 29.51, 28.80, 27.70, 26.31, 17.15, 16.40, 14.53. HRMS (ESI): Calcd for $C_{33}H_{42}NO_4$ $[M+H]^+$ 516.3114; Found: 516.3091.

ML20: White amorphous powder, yield 87%. ^{1}H NMR (400 MHz, $CDCl_3$) δ 7.40 (2H, dd, J = 8.1 Hz, 4.3 Hz), 7.28 (1H, d, J = 8.6 Hz), 7.03 (2H, t, J = 8.6 Hz), 6.93 (1H, dd, J = 8.5 Hz, 2.4 Hz), 6.89 (1H, s), 4.46 (1H, dd, J = 13.7 Hz, 7.7 Hz), 3.49 (1H, m), 3.40 (1H, t, J = 10.9 Hz), 2.88 (2H, m), 1.00 (3H, d, J = 6.7 Hz), 0.82 (3H, s), 0.80 (3H, d, J = 6.3 Hz). ^{13}C NMR (151 MHz, $CDCl_3$) δ 152.07, 148.20, 138.24, 138.13, 133.48, 126.25, 121.55, 120.39, 118.57, 115.87 (2C), 115.72 (2C), 109.32, 80.83, 66.89, 62.29, 55.34, 43.94, 41.65, 40.76, 39.89, 38.02, 31.56, 31.41, 30.31, 29.52, 28.80, 27.70, 26.31, 17.14, 16.40, 14.53. HRMS (ESI): Calcd for $C_{33}H_{41}FNO_4$ $[M+H]^+$ 534.3020; Found: 534.2998.

ML21: White amorphous powder, yield 83%. ^{1}H NMR (400 MHz, $CDCl_3$) δ 7.32 (2H, d, J = 7.9 Hz), 7.29 (1H, d, J = 8.5 Hz), 7.13 (2H, d, J = 8.3 Hz), 6.93 (1H, dd, J = 8.4 Hz, 2.4 Hz), 6.90 (1H, d, J = 2.3 Hz), 6.83 (1H, s), 4.46 (1H, m), 3.49 (1H, dd, J = 10.7 Hz, 5.4 Hz), 3.40 (1H, t, J = 10.9 Hz), 2.88 (2H, m), 2.32 (3H, s), 1.00 (3H, d, J = 6.7 Hz), 0.82 (3H, s), 0.80 (3H, d, J = 6.4 Hz). ^{13}C NMR (151 MHz, $CDCl_3$) δ 151.95, 148.32, 138.15, 137.96, 134.90, 133.36, 129.63 (2C), 126.20, 121.62, 118.72 (2C), 118.65, 109.31, 80.84, 66.89, 62.30, 55.35, 43.95, 41.65, 40.77, 39.90, 38.03, 31.57, 31.41, 30.31, 29.52, 28.81, 27.71, 26.32, 20.78, 17.15, 16.40, 14.53. HRMS (ESI): Calcd for $C_{34}H_{44}NO_4$ $[M+H]^+$ 530.3270; Found: 530.3267.

ML22: White amorphous powder, yield 81%. ^{1}H NMR (400 MHz, $CDCl_3$) δ 7.86 (1H, m), 7.25 (4H, m), 7.11 (1H, t, J = 7.5 Hz), 6.95 (1H, m), 6.91 (1H, s), 6.74 (1H, s), 4.46 (1H, m), 3.49 (1H, dd, J = 10.5 Hz, 4.2 Hz), 3.40 (1H, t, J = 10.9 Hz), 2.87 (2H, m), 2.67 (2H, q, J = 7.5 Hz), 1.00 (3H, d, J = 6.7 Hz), 0.82 (3H, s), 0.80 (3H, d, J = 6.3 Hz). ^{13}C NMR (151 MHz, $CDCl_3$) δ 152.37, 148.38, 138.16, 137.97, 134.79, 133.24, 128.55, 126.88, 126.21, 124.71, 121.58, 121.29, 118.60, 109.30, 80.84, 66.89, 62.31, 55.36, 43.95, 41.65, 40.77, 39.91, 38.03, 31.58, 31.42, 30.32, 29.52, 28.81, 27.72, 26.31, 24.21, 17.15, 16.41, 14.53, 13.96. HRMS (ESI): Calcd for $C_{35}H_{46}NO_4$ $[M+H]^+$ 544.3427; Found: 544.3416.

ML23: White amorphous powder, yield 85%. ^{1}H NMR (400 MHz, $CDCl_3$) δ 7.36 (2H, d, J = 8.7 Hz), 7.28 (1H, s), 6.93 (1H, dd, J = 8.4 Hz, 2.4 Hz), 6.88 (3H, m), 6.78 (1H, s), 4.46 (1H, m), 3.49 (1H, dd, J = 11.0 Hz, 5.6 Hz), 3.39 (1H, t, J = 10.9 Hz), 2.89 (2H, m), 1.00 (3H, d, J = 6.7 Hz), 0.82 (3H, s), 0.80 (3H, d, J = 6.3 Hz). ^{13}C NMR (151 MHz, $CDCl_3$) δ 156.15, 152.19, 148.37, 138.14, 137.93, 130.57, 126.19, 121.61, 120.54, 118.64, 114.33, 109.31, 80.84, 66.89, 62.30, 55.50, 55.35, 43.95, 41.65, 40.77, 39.90, 38.03, 31.57, 31.41, 30.31, 29.71, 29.52, 28.81, 27.71, 26.31, 17.15, 16.40, 14.53. HRMS (ESI): Calcd for $C_{34}H_{44}NO_5$ $[M+H]^+$ 546.3219; Found: 546.3217.

4.6. Biochemical studies

4.6.1. Oxygen-glucose deprivation-reperfusion (OGD/R)

The cells were pretreated with **ML5** for 2 h and then exposed to OGD medium (glucose-free Dulbecco's Modified Eagle medium), then placed in an anaerobic chamber containing 92% N_2, 3% O_2 and 5% CO_2 for 4 h at 37 °C. OGD was terminated by removing glucose-free medium and exposed to high-glucose medium and cell cultures were reintroduced to the regular CO_2 incubator at 37 °C for 2 h. Control cells were incubated in the high-glucose medium at 37 °C in a regular 74% N_2, 21% O_2 and 5% CO_2 incubator.

4.6.2. Cholinesterases (ChEs) activity assay

Male ICR mice (5–6 weeks old, about 18–22 g) were purchased from Shanghai Sippr-bk Laboratory Animal co, Ltd (Shanghai, China). In the

ChEs activity inhibition test, the animals are grouped as follows:

Group	Drugs and Doses	Number of mice
Control group	Normal saline	6
Rivastigmine group	Rivastigmine, 2 mg/kg	6
ML5-15 min group	ML5, 15 mg/kg	6
ML5-30 min group		6
ML5-45 min group		6
ML5-3 h group		6
ML5-12 h group		6

The mice cortex was homogenized in cold 75 mM sodium phosphate buffer (pH 7.4). The assay solution consisted of 50 μL of 0.1 mM phosphate buffer (pH 7.4), 100 μL of deionized water, 20 μL of mice cortex homogenate, and 30 μL of 2 mM acetylthiocholine iodide (Sigma; cat#01480) as the substrate of the ChEs enzymatic reaction, respectively. After reaction at 37 °C for 8 min, 50 μL 3% SDS was added to stop the reaction. Finally, after adding 50 μL of 0.2% 5,5′-dithiobis (2-nitrobenzoic acid) (DTNB, Sigma; cat#D8130), the ChEs assay was measured with a microplate reader (Biotek Instruments, Inc) at 440 nm and at least three independent runs were performed for each sample.

4.6.3. *ML5 prevented the loss of cell viability and reduced ROS levels in SH-SY5Y cells exposed to H_2O_2*

Human dopaminergic neuroblastoma SH-SY5Y cells (American Type Culture Collection, Virginia, USA) were cultured in Dulbecco's modified Eagle's medium (DMEM)/F-12 HAM nutrient medium (1:1 mixture) supplemented with 10% fetal bovine serum (FBS), penicillin (1000 units/mL), cultured in a 5% CO_2 three-gas incubator (Thermo Scientific) at 37 °C.

The viability of SH-SY5Y cells was analyzed by using the 3-(4,5-dimethylthiazol-2-yl)-2,5-diphenyltetrazolium bromide (MTT, Sigma; cat#M2128) assay. SH-SY5Y cells growing to the fusion state were laid on the 96-well plate at a concentration of $5*10^4$/mL. In order to test the ability of **ML5** in preventing the oxidative damage triggered by H_2O_2, a pretreatment with **ML5** (dissolved in DMSO) at 0.01–100 μM for 2 h and 200 μM H_2O_2 for another 24 h was performed in SH-SY5Y cells. Then 10 μL MTT (5 mg/ml) was added to the cells. The cells incubated for another 4 h at 37 °C. Subsequently, the medium was replaced with DMSO in each well. Finally, the absorbance was measured at 490 nm by a microplate reader (BioTek Instruments, Inc). The experiment was repeated three-five times. Graph Pad Prism and SPSS software was used for statistical analysis and all the results were expressed as mean ± standard error (SEM).

The intracellular production of ROS was assessed by the nonpolar compound 2′-7′-dichlorodihy drofluorescein diacetate (DCFH-DA, Sigma; cat#D6883). The DCFH-DA was diluted to 10 μM with medium. The cells were pretreatment with **ML5** for 2 h and loaded with 10 μM DCFH-DA. After this, washed cells three times with PBS to remove excess DCFH-DA and changed to fresh medium. Then the cells were stimulated with 200 μm H_2O_2 for 30 min. The conversion of DCFH-DA to the fluorescent product DCF was quantified using microplate reader (BioTek Instruments, Inc) (Em/Ex = 535/485 nm) and qualitatively observed using a fluorescence microscope (Nikon, Tokyo, Japan). All the experiments were repeated three times independently.

4.6.4. GSH and SOD assays

Cells or brain cortex were lysed. The total GSH was measured by a commercially available Total Glutathione Assay kit (Nanjing Jiancheng Bioengineering Institute, Nanjing, China; cat#A006-2-1). The SOD activity was detected by using SOD Assay Kit (WST-8 method) obtained from Beyotime (Beyotime Institute of Biotechnology, Nantong, China; cat#S0101M). All protocols completely complied to the manufacturer's instructions. The absorbance was assessed at 450 nm using a microplate reader. The absorbance was assessed at 405 nm (GSH) and 450 nm (SOD) using a microplate reader. The protein concentration was estimated by the Bicinchoninic Acid protein assay kit (Beyotime; cat#P0010). All the experiments were repeated three times independently.

4.6.5. *ML5 activated Nrf2 pathway in SY5Y cells*

Cytoplasmic and nuclear protein was extracted using the Nuclear and Cytoplasmic Protein Extraction Kit (Beyotime, Jiangsu, China; cat#P0028), respectively. The relative expression of cytoplasmic and nuclear Nrf2 protein were detected by western blot analysis.

4.6.6. Animal experiment

Male SD rats (6–8 weeks old, about 200–220 g) were purchased from Shanghai Sippr-bk Laboratory Animal Co, Ltd (Shanghai, China). They were housed in environmentally controlled conditions (temperature of 25 ± 2 °C, relative humidity of 60 ± 5%, and 12/12 h light/dark cycle). In the BCCAO experiment, the rats were divided into control group (sham group), model group (BCCAO group), low-dose **ML5** group (3 mg/kg), high-dose **ML5** group (15 mg/kg), and donepezil group (1 mg/kg) (n = 10, 13, 8, 12, 10 respectively).

The compound was pre-administered for 2 weeks. Before surgery, the animals fasted for 12 h. An intraperitoneal injection of 10% chloral hydrate (0.1 mL/100 g body weight) was used as anesthesia. Then, a midline incision of the neck was followed by blunt muscle dissection and the common carotid arteries were exposed. Then the para-arterial vagus nerve was separated with a glass minute needle. The same procedure was performed in the sham operation group rats without carotid artery occlusion.

The Morris water maze (MWM) test was performed at 28 days after the surgery. The maze was made of a circular tub (height 50 cm, diameter 180 cm) filled to a depth of 30 cm with water maintained at 25 ± 1 °C. Day 1: visual platform trial; Day 2–5: during the hidden platform trial, the rats were trained twice a day for 3 days. The training period was fixed every day. If the rats did not find the platform within 1 min, they were guided to find the platform and stayed on the platform for 10–15 s. Day 6: during the probe test, remove the platform and record the movement track of the rats and the escape latency. In the course of the experiment, the video acquisition system of AniLab Software Technology Co, Ltd. was used to record the mouse motion trajectory, and the AVIAS (Animal Video Iracking Analysis Systcm) software was used for trajectory analysis.

Part of rat brain samples were collected after perfusion with ice-cold fixative solution (0.1 M phosphate buffer (PB), pH 7.3 and 4% paraformaldehyde) for HE staining. First, after deparaffinization and rehydration, 4 μm paraffin sections were rinsed in distilled water and then stained with hematoxylin solution (Beyotime Biotechnology; cat#C0105S) for 8 min. Next, the sections were stained with eosin solution (Beyotime Biotechnology; cat#C0105S) for 3 min, followed by dehydration with graded alcohol and clearing in xylene. Finally, the sections were mounted using a synthetic resin.

4.6.7. Western blot

The animals were euthanized after BCCAO surgery, and part of brain samples were collected as fresh tissue for western blot. Similarly, after treatment, the SH-SY5Y cells were lysed with a lysis buffer and centrifuged, then supernatant was collected as total extracts. To prepare the cytoplasmic and nuclear fraction, cells were lysed using nuclear and cytoplasmic protein extraction kit (Beyotime; cat#P0028) according to the manufacturer's instructions. The brain homogenates and cell lysates were quantified with Bicinchoninic Acid protein assay kit (Beyotime; cat#P0010). The homogenates and lysates (30 μg protein) were fractionated by 10% SDS-PAGE and transferred to polyvinylidene fluoride membrane (PVDF, Millipore; cat#IPVH00010). After transfer, membranes were blocked in 5% skim milk and incubated overnight at 4 °C with primary antibody, and incubated with anti-rabbit or anti-mouse HRP antibody (1 : 2000 dilution) for 2 h at room temperature. A rabbit polyclonal antibody (1: 500 in Tris-buffered saline with Tween (TBST)) for Nrf2 (Proteintech; cat#16396-1-AP), a rabbit monoclonal

antibody for β-tubulin (Servicebio; cat#GB11017), a mouse monoclonal antibody for Pcna (abcam; cat#ab29) was used to detect the corresponding proteins. After peroxidase-conjugated goat anti-rabbit/anti-mouse secondary antibody (Santa Cruze; cat#sc-2004, cat#sc-2005) was used, ECL (Millipore) detection reagent was used for visualization according to the manufacturer's instructions. Densitometry analysis of the bands was performed using Image J software.

4.6.8. Statistical analysis

All the results were expressed as mean ± standard error (SEM). Image J program was used to analyze the density of western blot and immunofluorescence images. Graph Pad Prism 8.0 (GraphPad Software, La Jolla CA, USA) was used for data processing and IBM SPSS Statistics 25 (SPSS Inc., Chicago, IL) was used for statistical analysis. The two-way ANOVA was used to determine the statistical significance ($p < 0.05$) of the MWM data. A one-way ANOVA followed by Student's *t*-test (non-parametric Mann-Whitney and Wilcoxon tests) were used to determine the statistical significance ($p < 0.05$) of the other obtained data.

4.6.9. Molecular docking studies

The crystal structures of hAChE (PDB ID: 6F25) and Keap1 (PDB ID: 3VNH) were downloaded from the Protein Data Bank (https://www.rcsb.org/) as receptors. Maestro 10.5 embedded in Schrödinger software package (2016-1) was employed to perform all molecular modeling studies. Protein structures of hAChE and Keap1 were refined by Protein Preparation Wizard. Protein energies were minimized with Root Mean Square Deviation (RMSD) value of 0.3 Å using OPLS-2005 force field. LigPred was used to prepare 3D conformations of ligands (**ML5** and rivastigmine). Epik generated the protonation states of **ML5** and rivastigmine at pH values from 5.0 to 9.0. Docking sites were centered by original ligands complexed with hAChE and Keap1 The grid boxes of receptors were set to 20 Å to accommodate all ligand atoms. Then the Glide extra precision (XP) model was utilized to dock all refined ligands to the active sites of receptors. Binding affinities between the most superior conformers of ligands and the receptors were calculated by Prime MM-GBSA under VSGB solution model using OPLS-2005 force field. Interaction model figures were generated by PyMOL.

4.6.10. Acute toxicity study.

All animal experiments were carried out in accordance with the National Institutes of Health Guide for the Care and Use of Laboratory Animals of China for animal experimentation, and were approved by the Animal Ethics Committee of the East China University of Science and Technology. A total of 14 healthy male mice (20–30 g) were randomly divided into 2 groups for acute toxicity study of the compound **ML5**. These animals were left without food for 12 h before the experiment. Compound **ML5** was suspended in normal saline and given orally to divided into 2 groups, including 0 and 500 mg/kg, n = 7 per group. After the administration of the test compound, the mice were observed closely for the first 4 h for the behavior and mortality.

Then, each animal was weighed every day, and recorded the mortality. After 2 weeks, the animals were sacrificed to observe the changes in the heart, liver, and kidneys.

Declaration of Competing Interest

The authors declare that they have no known competing financial interests or personal relationships that could have appeared to influence the work reported in this paper.

Acknowledgments

This work was supported by the National Natural Science Foundation of China (Grants 81973196 and 81673318), the 111 Project (Grant BP0719034) and the Natural Science Foundation of Shanghai (Grant 19ZR1413900).

Appendix A. Supplementary material

Supplementary data to this article can be found online at https://doi.org/10.1016/j.bmc.2021.116109.

References

1 Elahi FM, Miller BL. A clinicopathological approach to the diagnosis of dementia. *Nature Rev Neurol*. 2017;13:457–476. https://doi.org/10.1038/nrneurol.2017.96.
2 O'Brien JT, Thomas A. Vascular dementia. *Lancet*. 2015;386:1698–1706. https://doi.org/10.1016/S0140-6736(15)00463-8.
3 Wu Y, Zhou Q, Zhang T, et al. Discovery of potent, selective, and orally bioavailable inhibitors against phosphodiesterase-9, a novel target for the treatment of vascular dementia. *J Med Chem*. 2019;62:4218–4224. https://doi.org/10.1021/acs.jmedchem.8b01041.
4 Bartus RT, Dean RL, Beer B, Lippa AS. The cholinergic hypothesis of geriatric memory dysfunction. *Science*. 1982;217:408–414. https://doi.org/10.1126/science.7046051.
5 Perry EK, Walker MP, Grace J, Perry R. Acetylcholine in mind: a neurotransmitter correlate of consciousness? *Trends Neurosci*. 1999;22:273–280. https://doi.org/10.1016/S0166-2236(98)01361-7.
6 Happich M, Kirson NY, Desai U, et al. Excess costs associated with possible misdiagnosis of alzheimer's disease among patients with vascular dementia in a Uk Cprd population. *Alzheimer's Dementia*. 2014;10:911–912. https://doi.org/10.1016/j.jalz.2014.07.110.
7 Dembitsky VM, Dzhemileva L, Gloriozova T, D'yakonov V. Natural and synthetic drugs used for the treatment of the dementia. *Biochem Biophys Res Commun*. 2020;524:772–783. https://doi.org/10.1016/j.bbrc.2020.01.123.
8 Emre M, Aarsland D, Albanese A, Byrne EJ, Deuschl G, De Deyn PP, et al. Rivastigmine for dementia associated with Parkinson's disease. *N Engl J Med*. 2004;24:2509–2518. https://doi.org/10.1056/NEJMoa041470.
9 de la Torre JC. Vascular risk factor detection and control may prevent Alzheimer's disease. *Ageing Res Rev*. 2010;9:218–225. https://doi.org/10.1016/j.arr.2010.04.002.
10 Lin MS, Chiu MJ, Wu YW, et al. Neurocognitive improvement after carotid artery stenting in patients with chronic internal carotid artery occlusion and cerebral ischemia. *Stroke*. 2011;42:2850–2854. https://doi.org/10.1161/STROKEAHA.111.613133.
11 Peng S, Zhang B, Meng X, Yao J, Fang J. Synthesis of piperlongumine analogues and discovery of nuclear factor erythroid 2-related factor 2 (Nrf2) activators as potential neuroprotective agents. *J Med Chem*. 2015;58:5242–5255. https://doi.org/10.1021/acs.jmedchem.5b00410.
12 Fishbein JC, Holland R. Chemistry of the cysteine sensors in Keap1. *Antioxid Redox Signal*. 2010;13:1749–1761. https://doi.org/10.1089/ars.2010.3273.
13 Uruno A, Furusawa Y, Yagishita Y, et al. The Keap1-Nrf2 system prevents onset of diabetes mellitus. *Mol Cell Biol*. 2013;33:2996–3010. https://doi.org/10.1128/MCB.00225-13.
14 Benchekroun M, Romero A, Egea J, et al. The antioxidant additive approach for Alzheimer's disease therapy: new ferulic (lipoic) acid plus melatonin modified tacrines as cholinesterases inhibitors, direct antioxidants, and nuclear factor (Erythroid-Derived 2)-Like 2 activators. *J Med Chem*. 2016;59:9967–9973. https://doi.org/10.1021/acs.jmedchem.6b01178.
15 Zhang M, An C, Gao Y, Leak RK, Chen J, Zhang F. Emerging roles of Nrf2 and phase II antioxidant enzymes in neuroprotection. *Prog Neurobiol*. 2013;100:30–47. https://doi.org/10.1016/j.pneurobio.2012.09.003.
16 Bolognesi ML, Cavalli A, Valgimigli L, et al. Multi-target-directed drug design strategy: from a dual binding site acetylcholinesterase inhibitor to a trifunctional compound against Alzheimer's disease. *J Med Chem*. 2007;50:6446–6449. https://doi.org/10.1021/jm701225u.
17 Cavalli A, Bolognesi ML, Minarini A, et al. Multi-target-directed ligands to combat neurodegenerative diseases. *J Med Chem*. 2008;51:347–372. https://doi.org/10.1021/jm7009364.
18 Yang GX, Huang Y, Zheng LL, et al. Design, synthesis and evaluation of diosgenin carbamate derivatives as multitarget anti-Alzheimer's disease agents. *Eur J Med Chem*. 2019;187, 111913. https://doi.org/10.1016/j.ejmech.2019.111913.
19 Pan H, Van Khang P, Dong D, Wang R, Ma L. Synthesis and SAR study of novel sarsasapogenin derivatives as potent neuroprotective agents and NO production inhibitors. *Bioorg Med Chem Lett*. 2017;27:662–665. https://doi.org/10.1016/j.bmcl.2016.11.070.
20 Yang GX, Ge SL, Wu Y, et al. Design, synthesis and biological evaluation of 3-piperazinecarboxylate sarsasapogenin derivatives as potential multifunctional anti-Alzheimer agents. *Eur J Med Chem*. 2018;156:206–215. https://doi.org/10.1016/j.ejmech.2018.04.054.
21 Kinarivala N, Patel R, Boustany RM, Al-Ahmad A, Trippier PC. Discovery of aromatic carbamates that confer neuroprotective activity by enhancing autophagy and inducing the anti-apoptotic Protein B-cell lymphoma 2 (Bcl-2). *J Med Chem*. 2017;60:9739–9756. https://doi.org/10.1021/acs.jmedchem.7b01199.
22 Poprac P, Jomova K, Simunkova M, Kollar V, Rhodes CJ, Valko M. Targeting free radicals in oxidative stress-related human diseases. *Trends Pharmacol Sci*. 2017;38:592–607. https://doi.org/10.1016/j.tips.2017.04.005.
23 Kobayashi M, Yamamoto M. Nrf2–Keap1 regulation of cellular defense mechanisms against electrophiles and reactive oxygen species. *Adv Enzyme Regul*. 2006;46:113–140. https://doi.org/10.1016/j.advenzreg.2006.01.007.

24 Du SQ, Wang XR, Xiao LY, et al. Molecular mechanisms of vascular dementia: what can be learned from animal models of chronic cerebral hypoperfusion? *Mol Neurobiol*. 2017;54:3670–3682. https://doi.org/10.1007/s12035-016-9915-1.
25 Leon-Moreno LC, Castaneda-Arellano R, Rivas-Carrillo JD, Duenas-Jimenez SH. Challenges and improvements of developing an ischemia mouse model through bilateral common carotid artery occlusion. *J Stroke Cerebrovasc Dis*. 2020;29, 104773. https://doi.org/10.1016/j.jstrokecerebrovasdis.2020.104773.
26 Kensler TW, Wakabayashi N, Biswal S. Cell survival responses to environmental stresses via the Keap1-Nrf2-ARE pathway. *Annu Rev Pharmacol Toxicol*. 2007;47: 89–116. https://doi.org/10.1146/annurev.pharmtox.46.120604.141046.
27 Vitorovic-Todorovic MD, Koukoulitsa C, Juranic IO, Mandic LM, Drakulic BJ. Structural modifications of 4-aryl-4-oxo-2-aminylbutanamides and their acetyl- and butyrylcholinesterase inhibitory activity. Investigation of AChE-ligand interactions by docking calculations and molecular dynamics simulations. *Eur J Med Chem*. 2014; 81:158–175. https://doi.org/10.1016/j.ejmech.2014.05.008.
28 Zueva I, Dias J, Lushchekina S, et al. New evidence for dual binding site inhibitors of acetylcholinesterase as improved drugs for treatment of Alzheimer's disease. *Neuropharmacology*. 2019;155:131–141. https://doi.org/10.1016/j.neuropharm.2019.05.025.
29 Lo SC, Li X, Henzl M, Beamer LJ, Hannink M. Structure of the Keap1:Nrf2 interface provides mechanistic insight into Nrf2 signaling. *EMBO J*. 2006;25:3605–3617. https://doi.org/10.1038/sj.emboj.7601243.
30 Heightman TD, Callahan JF, Chiarparin E, et al. Structure-activity and structure-conformation relationships of aryl propionic acid inhibitors of the Kelch-like ECH-Associated Protein 1/Nuclear Factor Erythroid 2-Related Factor 2 (KEAP1/NRF2) protein-protein interaction. *J Med Chem*. 2019;62:4683–4702. https://doi.org/10.1021/acs.jmedchem.9b00279.